ABSTRACT

DREW PATRICK TURNER. Analysis of Taxi Test Data for an Unmanned Aerial Vehicle Implemented with Fluidic Flow Control. (Under the direction of Dr. Charles E. Hall, Jr.)

Serpentine inlet ducts are utilized in many aircraft where the inlet capture area is located off the thrust line or there is a desire to conceal the engine compressor face. Due to the curvature that characterizes a compact serpentine duct, issues with flow distortion and total pressure loss at the engine face arise leading to reduction in propulsion system performance. Computational analysis has shown that flow control implementing micro-fluidic vortex generators significantly reduces the losses. Previous work at North Carolina State University has demonstrated the benefits of a fluidic flow control of this type in a highly compact serpentine inlet duct through the design and experimental static testing of a propulsion system for an uninhabited aerial vehicle. With the implementation of flow control, engine face distortion was reduced and propulsion system performance was increased. This work continues the investigation of the effectiveness of the fluidic flow control by examining the performance of the system during dynamic situations through high speed taxi testing of an uninhabited aerial vehicle implemented with this technology. Additionally, the collected data was used to compare calculated takeoff parameters to values calculated using standard takeoff analysis.

ANALYSIS OF TAXI TEST DATA FOR AN UNMANNED AERIAL VEHICLE IMPLEMENTED WITH FLUIDIC FLOW CONTROL

By

DREW PATRICK TURNER

A thesis submitted to the Graduate Faculty of
North Carolina State University
In partial fulfillment of the
Requirements for the degree of

Master of Science

AEROSPACE ENGINEERING

Raleigh, NC
2006

APPROVED BY:

Dr. Charles E. Hall, Jr. **Advisory Committee Chairman**	**Dr. Ashok Gopalarathnam** **Advisory Committee Member**

Dr. Sharon Lubkin
Advisory Committee Member

DEDICATION

I would like to dedicate this research and the whole of my college career to my parents, Gregory and Patricia Turner. With their love and support I have become the person I am today.

BIOGRAPHY

Drew Patrick Turner was born in Jacksonville, FL on April 1, 1982 to Gregory and Patricia Turner. As a part of a military family, he and his younger siblings, Bryce and Casey, grew up in many different areas around the world. Finally settling in Fayetteville, North Carolina in 1994, he graduated from South View High School in 2000. In May of 2004, he graduated from North Carolina State University with a Bachelor of Science Degree in Aerospace Engineering. In the fall of 2004, Drew began work on his Master of Science degree in Aerospace Engineering as a part of the Flight Research Program at North Carolina State University. Also in the fall of 2004, he was selected as participant in the United States Air Force Technical Degree Sponsorship Program. Upon completion of this degree, Drew will attend Officer Training School at Maxwell AFB in Alabama where he will be commissioned as a 2^{nd} Lieutenant in the United States Air Force as a Developmental Engineer in the field of Aeronautical Engineering.

ACKNOWLEDGMENTS

First of all I would like to thank my advisor Dr. Charles E. Hall, Jr. and Mr. Stearns B. Heinzen for their guidance throughout my graduate career at North Carolina State University. I would also like to thank my committee members Dr. Ashok Gopalarathnam and Dr. Sharon Lubkin.

In addition, I would like to thank Mr. Robert Vess, who piloted the aircraft during the taxi test and the personnel at the Harnett County Airport for their cooperation and hospitality during our testing activities. I would also like to express my gratitude to Wallis Collie for the ground work he laid at NC State in this field of research. A special thanks to my colleague, Mr. David Roberts, who was of great assistance during the project and graduate school. Finally, I would like to extend my appreciation to family and friends for their support during my schooling at North Carolina State University.

TABLE OF CONTENTS

LIST OF FIGURES

LIST OF TABLES

LIST OF SYMBOLS

a_x	Acceleration in X-direction
a_y	Acceleration in Y-direction
a_z	Acceleration in Z-direction
b	Wing Span
AR	Aspect Ratio
C_D	Total Drag Coefficient
C_{Do}	Minimum Drag Coefficient
C_i	Calibration Coefficient
C_L	Lift Coefficient
$C_{L,max}$	Maximum Lift Coefficient
D	Drag
e	Oswald Efficiency Factor
g	Gravitational Constant
L	Lift
P_x	Measured Pressure
PAV	Ring Average Total Pressure
$PAVLOW$	Average Total Pressure of Low Total Pressure Region for a Ring
$PFAV$	Face Average Total Pressure
p	Roll Rate
p_{atm}	Atmospheric Pressure
p_0	Rake Port Total pressure
p_{static}	Static Pressure
q	Pitch Rate
$\bar{q}$	Dynamic Pressure
r	Yaw Rate
RPM	Rotor Speed/Revolutions per Minute
s_{LO}	Takeoff Distance
s_L	Landing Distance
S	Wing Planform Area
T	Thrust
T_i	Idle Thrust
V_{LO}	Lift Off Velocity
V_{stall}	Stall Velocity
V_{TD}	Touch down Velocity
V_x	Transducer Voltage at P_x
V_{meas}	Measured Airspeed
V_{wind}	Wind Velocity
$V_{x,wind}$	Headwind Component
$V_{y,wind}$	Crosswind Component
W	Weight
α	Angle of Attack
β	Angle of Sideslip
θ	Pitch Angle

θ_i	Circumferential Location
$\bar{\theta}_i$	Circumferential Extent Element
μ_r	Rolling Coefficient of Friction
μ_b	Braking Coefficient of Friction
ρ_∞	Density
Φ	Bank Angle
$\left(\frac{\Delta PC}{P}\right)_i$	Circumferential Intensity
$\left(\frac{\Delta PR}{P}\right)_i$	Radial Intensity

1 Introduction

As the roles of uninhabited aerial vehicles (UAVs) have become more advanced, their designs are becoming more compact and complex to meet "survivability, affordability, and low drag constraints."[1,2] Several different technologies have been developed to satisfy these needs. The technology of interest in this work is the highly compact serpentine inlet duct, or S-duct. S-ducts are employed on aircraft with the inlet ducts that are located off the thrust line and in applications when there is a need for the engine compressor face to be concealed. Highly compact serpentine inlet ducts provide advantages over traditional S-ducts. By shortening the inlet, the overall aircraft length can be reduced. A shorter aircraft requires less material, resulting in lower weight and cost. Reduced weight results in a higher performance compact aircraft.[3] A compact S-duct is characterized by its extreme wall curvature as exhibited in Figure 1-1.

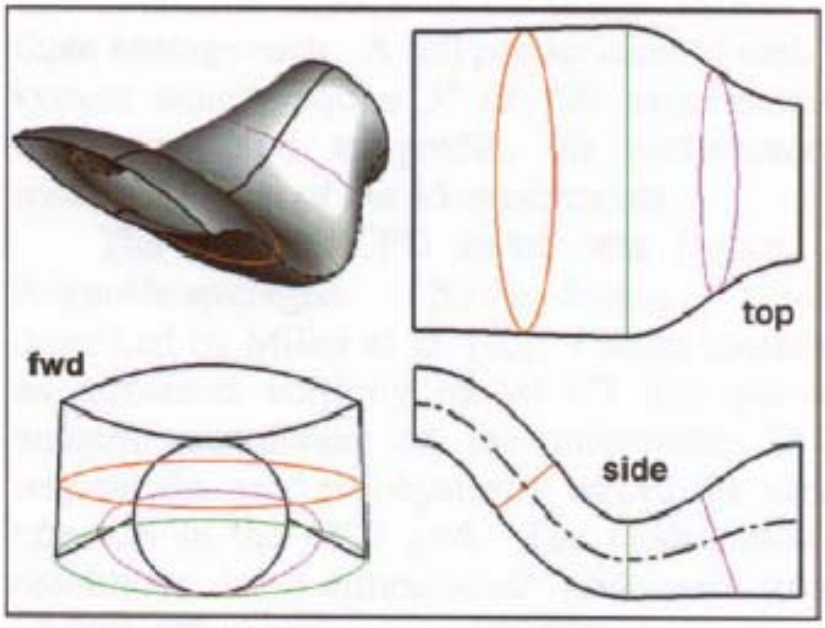

Figure 1-1: Typical Serpentine Inlet Duct (S-Duct)[4]

Due to the aggressive curves of the inlet duct, issues with pressure losses at the engine face, inlet flow distortion and separation arise. These problems can lead to performance reduction in the propulsion system, as well as reduced engine life.[5] Several different approaches have been developed to alleviate these issues including different variations of vortex generators (VGs) in the inlet duct. One promising method, currently being researched, is an active flow control implementing micro-fluidic VGs.

1.1 Previous Work in Fluidic Flow Control

Previous work at NC State has demonstrated the advantages of implementing flow control with micro-fluidic VGs in a highly compact serpentine inlet duct. This work encompassed the design and experimental testing of a propulsion system for a turbojet powered UAV with fluidic flow control in a highly compact serpentine inlet duct.[5] Prior to this work, a majority of the investigations in to fluidic flow control in S-ducts were through computational analysis. The results from these analytical approaches were used to validate inlet flow patterns during experimental testing on the final system design.

The propulsion system designed for this project included a highly compact serpentine inlet duct, a turbojet engine, bleed air system, and exhaust pipe. The S-duct inlet was constructed with two manifolds that fed bleed air from the compressor of the engine to an array of micro-fluidic vortex generators discussed in the previous section. The engine used in the propulsion system was a modified Aviation Microjet Technology (AMT) AT1500 turbojet. A picture of the AT1500 can be seen in Figure 1-2 during one of its early tests. The engine was a prototype that weighed 20 lbs and was rated at 150 lbs of thrust.

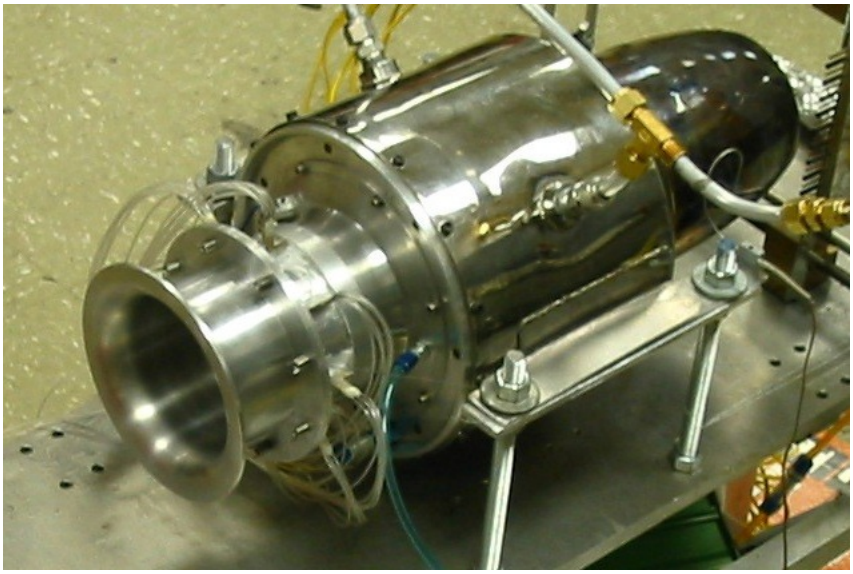

Figure 1-2: AMT AT1500 Turbojet[5]

Several modifications were made to the engine, including bleed air taps in the compressor section, removal of bellmouth for interfacing the inlet, and trimming of the exit nozzle for the addition of an extended exhaust pipe. The bleed air system supplied compressed air to the micro-fluidic VGs for flow control. The system consisted of copper tubing that piped air from the compressor section of the engine through the fuel tank for cooling and to the manifolds in the inlet duct via a solenoid valve for control of the bleed air. The exhaust pipe was a double walled concentric ejector configuration. The inner wall was tightly fitted around the engine exit and acted as the main exhaust pipe. The outer wall was slightly larger in diameter and length to enable ambient air to be entrained between the two walls for cooling.

To experimentally establish the propulsion system's performance, a build-up approach was employed.[6] Several static engine tests were conducted beginning with the baseline turbojet engine continuing with the addition of components until the final

configuration was reached. This approach allowed for performance losses to be attributed to individual components. Upon completion of the build-up test plan, the objectives of testing focused on establishing the extent of inlet flow distortion with and without flow control, and the effect of the flow control on the propulsion system's overall static performance.[5] The standards for testing and determining the extent of inlet flow distortion are outlined by Society of Automotive Engineers (SAE) Aerospace Recommended Practice (ARP) 1420 publication and will be discussed later in the Inlet Flow Distortion and Flow Control Analysis section. Results from the static testing provided a baseline for qualitative and quantitative comparison with the current work's results. The work by Collie[5] provides a more in depth discussion of the propulsion system design and experimental static engine testing results.

1.2 Present Work: Objectives

The purpose of this research is to continue the previous work conducted at NC State by investigating the performance of fluidic flow control in a dynamic setting and verify predicted takeoff parameters for the uninhabited aerial vehicle (UAV) incorporating with this technology. To collect data for this project, a series of high speed taxi runs were performed with the instrumented research vehicle. The data was analyzed and compared to the previous work conducted at North Carolina State University to evaluate the performance of the fluidic flow control. An analysis of takeoff performance on the test vehicle was also completed. Takeoff distances were calculated from the collected experimental data to determine accuracy of the values obtained using analytical takeoff performance analysis.

2 Experimental Taxi Testing

2.1 Overview of Taxi Tests and Objectives

The main goals for taxi testing the UAV were to determine the performance of the fluidic flow control in a dynamic setting, and to examine takeoff performance. Taxi testing also provided the opportunity for the pilot to test the aircraft's ground handling and allowed the testing support team to evaluate the UAV's systems and standard operating procedures in preparation for flight testing. All taxi tests were performed at the Harnett County Airport in Erwin, NC (Figure 2-1). With a main runway measuring 4,300 feet and a partial parallel taxi way there was ample room for both high and low speed taxi test operations. All the high speed taxi tests were conducted on Runway 5. The heading on that runway is 50° east of north. This was important when considering the contributions due to wind on test days.

Figure 2-1: Harnett County Airport

Low speed taxi testing was conducted to evaluate aircraft handling and the pneumatic braking system at safer speeds under the UAV's own power and to identify any problems that might be intensified at higher speeds.

The high speed taxi testing of the UAV provided the opportunity to analyze the inlet flow control at near flight operating conditions. High speed taxi testing included four runs at aircraft acceleration lengths of 250 ft and 375 ft. For each distance a run was made with and without flow control. Data was collected from the array of instrumentation for all runs. During the high speed taxi tests, airspeeds were monitored via wireless modem. A "knock-off" velocity was established as a 10% safety margin on the stall speed for to avoid an accidental takeoff. By monitoring the airspeed, changes could be made to the test plan without scratching the whole test day. The complete UAV Taxi Test Plan can be found in Appendix A.

2.2 Test UAV Description

The UAV used for this research was designed and built specifically as a technology demonstrator. The airframe of the test vehicle was comprised of composite materials including fiberglass, carbon fiber, and Korex. The aircraft was a highly swept flying wing with a diamond delta planform and single vertical tail. The wingspan and length of the UAV were 8 feet and 10 feet, respectively. The vehicle was remotely piloted by line-of-sight and had a takeoff weight of 214 lbs during taxi testing. The test vehicle was supported by fully retractable tricycle landing gear with a steerable nose gear and pneumatic brake system on the main gear. The propulsion system discussed in the previous work was installed in the aircraft for dynamic testing. A detailed account of aircraft integration of the system can be found in the work by W.V. Collie.[5]

2.3 Instrumentation and Data Collection

The purpose of any experimental test plan is to collect high quality useful data.[7] The UAV used during experimental testing in this project was instrumented with an array of transducers to measure dynamic flight and pressure data. All transducers in the aircraft were interfaced with a centralized flight computer that was responsible for data capture, real-time monitoring and stability augmentation system implementation. Below in Table 2-1 is a listing of the critical instrumentation and data the flight computer was configured to collect during taxi testing. Each of the instruments will be discussed further in the following sections.

For taxi test purposes, the NCSU pitot-static probe was used in lieu of the Space Age Control Mini Air Data Boom because the risk of losing the instrument was considered unnecessary by the test coordinator and support team. Angle of attack of the aircraft for the aircraft was 0° and angle of sideslip was estimated from weather conditions and pitot-static data.

Table 2-1: Taxi Test Critical Instrumentation and Data Captured

Sensor	Quantity Measured		Range
NCSU Pitot-Static Probe	Dynamic Pressure	$\bar{q}$	0-5 psi
	Static Pressure	p_{static}	0-5 psi
OR			
Space Age Control Mini Air Data Boom	Dynamic Pressure	$\bar{q}$	0-5 psi
	Static Pressure	p_{static}	0-5 psi
	Angle of Attack (AOA)	α	+/- 30° (+/- π/6 rads)
	Angle of Sideslip (AOS)	β	+/- 30° (+/- π/6 rads)
AND			
Crossbow VG400CC IMU	Angles	θ, Φ	+/- 180° (+/- π rads)
	Angular Rates	p,q,r	+/- 200 deg/sec (+/- 10 π /9 rads/sec)
	Linear Accelerations	a_x, a_y, a_z	+/- 10 g
PSI ESP-64 Module	Inlet Rake – Total Pressures		+/- 5 psi
Pressure Transducers	Manifold Pressures		0-30 psi
AMT 1500 ECU	Exhaust Gas Temperature	EGT	
	Rotor Speed	RPM	
Aircraft Transmitter and Receiver	Pilot Commands	Throttle, Brakes, surface deflections, etc.	

2.3.1 Flight Computer

The on-board flight computer used for data collection and real-time control system implementation was the NCSU Flight Research LINUX In-Flight Testing (LIFT) system (Figure 2-2). The LIFT computer is a PC104 based system that provides the flexibility and capability to be utilized in a variety of flight testing programs.[8] The LIFT computer has been used in several previous research projects conducted by NCSU including flight testing of a modified C-130A Hercules, and controller verification on Flight Research's Stingray and Vortex UAVs. The system allowed for real-time observation of critical data during the high speed taxi runs and necessary adjustments to the aircraft's controllers via wireless modem. All data was collected at a sampling rate of 50 Hz.

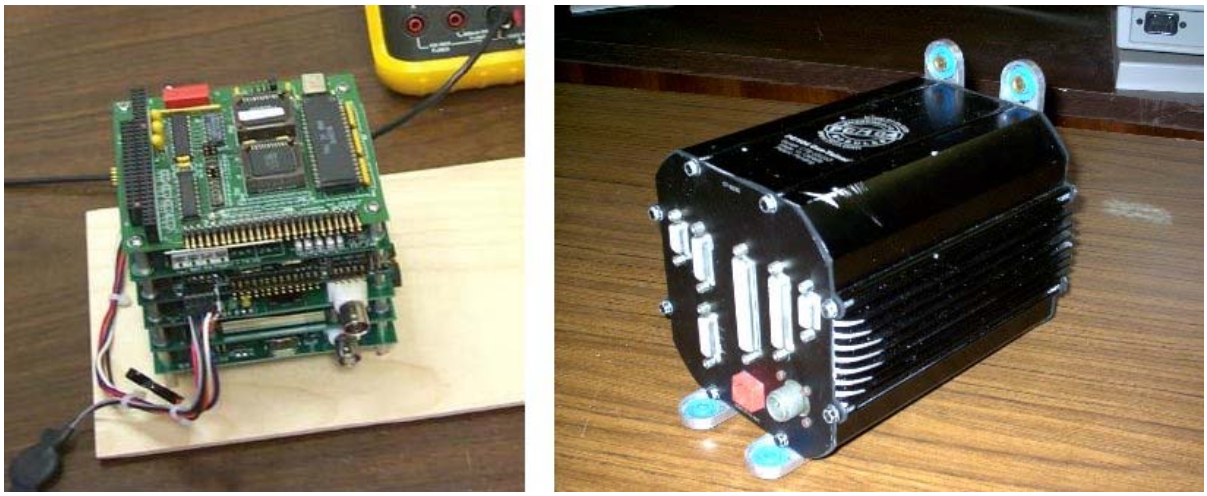

Figure 2-2: LIFT PC104 Stack and LIFT Computer

The collected data was written to four different files: XD, PSI, RC, and SAS. The files were formatted as MATLAB® compatible arrays to ease the transition into data post-processing. The XD files contain the data from each transducer including the Crossbow, the pitot-static tube, manifold pressures, and engine RPM. The PSI files stored pressure

information from the inlet rake connected to the ESP-module. The RC and SAS files were a record of the inputs from the pilot and the stability augmentation system, respectively.

All the data reduction was performed using scripts written in MATLAB®. The programs applied the appropriate calibrations and corrections to the raw taxi test data. A copy of the scripts can be found in Appendix B accompanied with commenting and units for the collected data.

2.3.2 Crossbow VG400

To measure the aircraft rates and accelerations the Crossbow VG400CC Inertial Measurement Unit (IMU) was used. The VG400 is capable of full six-degree-of-freedom dynamic measurements including linear accelerations along the UAV's body axes: a_x, a_y, and a_z, and angular rates: roll rate (p), pitch rate (q), and yaw rate (r). Three micro-machined accelerometers and rate sensors within the Crossbow measure these quantities. Figure 2-3 illustrates the orientation of the aircraft's axes and positive directions of the measured quantities.

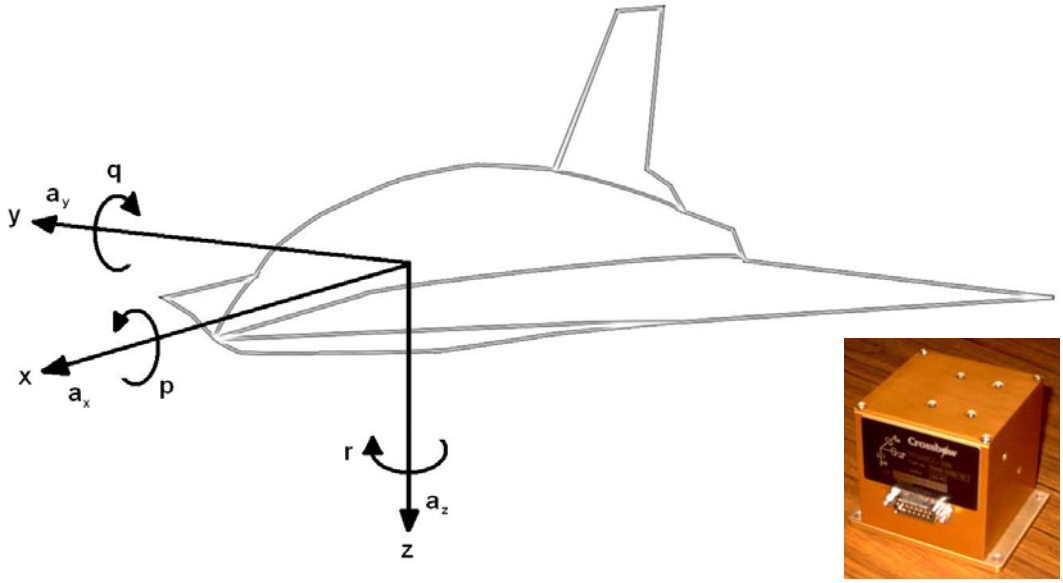

Figure 2-3: Aircraft Coordinate System (arrows denote (+) direction)
(Inset: Crossbow VG400CC)

To make use of the full capabilities of the VG400, it was run in *Angle Mode*. In this mode, the pitch (θ) and bank (Φ) angles are integrated from the angular rates and the accelerations the raw voltages from the accelerometers. The angles follow the same notation as the rates from which they are integrated. A conversion provided by the manufacturer was used to convert the voltages to accelerations. The units of output for the angular rates and the angles were degrees per second and degrees, respectively. These were converted to radians for analysis. The IMU was mounted near the center gravity (CG) of the aircraft as recommended by the VG400 Manual to eliminate the "lever effect," that would skew the measured aircraft accelerations.[9]

2.3.3 Inlet Pressure Measurement System

The inlet pressure measurement system was comprised of a 40 port total pressure inlet rake and Pressure Systems Inc. (PSI) ESP-64HD miniature pressure scanner (Figure 2-4). This system is the same one used during the static engine tests of the previous work. The pressure scanner communicated with the LIFT computer through NCSU Flight research designed interface to record total pressures at the engine face.

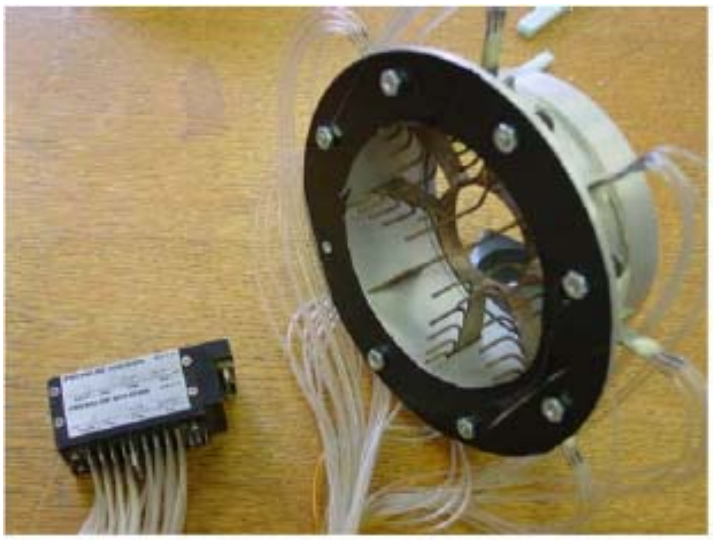

Figure 2-4: PSI ESP Pressure Transducer and Inlet Rake[5]

1.1.1.1 Inlet Total Pressure Rake

The inlet total pressure rake was designed and built to specifications in SAE ARP 1420. The rake was located at the aerodynamic interface plane (AIP) of the inlet/engine face, or the exit plane of the inlet for this propulsion system, and only accounted for 8% total blockage of inlet area.[5] The AIP is the plane used to define distortion and performance at the interface of the engine and inlet.[10] The inlet rake had five rings with eight ports on each ring located at the centroids of equal areas across the AIP. Figure 2-5 displays the nomenclature

for the ports on each ring and rake. Ring 1 is the inner most ring progressing in consecutive order towards the outer ring. The top most rake is Rake 1 with the rake index increasing in the clockwise direction with engine facing forward.

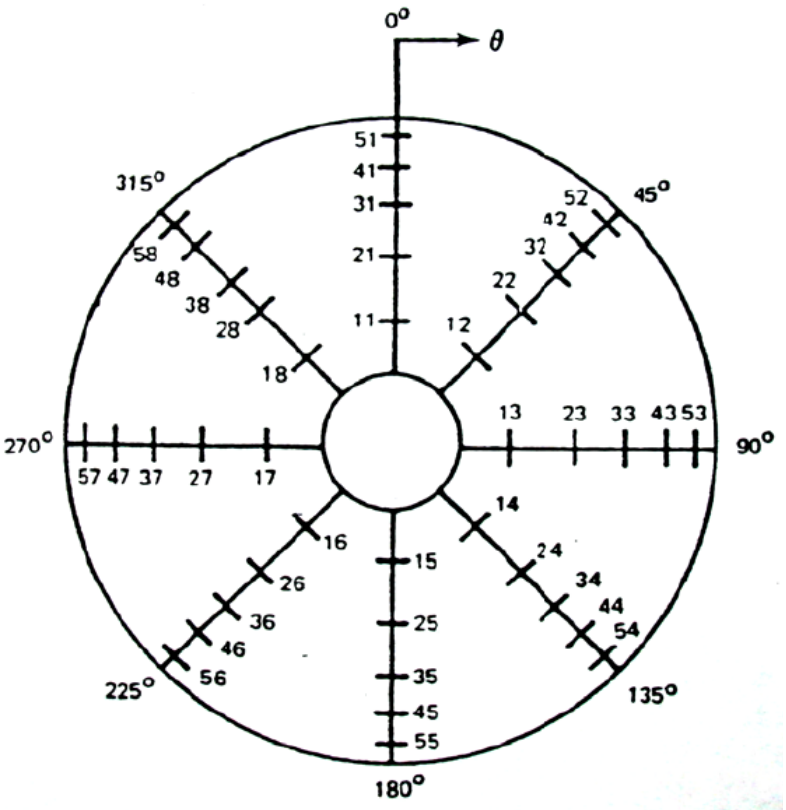

Figure 2-5: Inlet Rake Port Nomenclature – View Looking Forward[10]
(Port 35 = Ring 3, Rake 5)

1.1.1.2 PSI ESP-64HD Module

This project made use of the first 40 addressed ports of the PSI ESP-64HD miniature pressure scanner. Each individual port was associated with a silicon transducer capable of reading pressures in a range of +/-5 pounds per square inch. For each transducer, a fourth-order calibration curve (Eq. 1) was used to convert voltages to pressures, where P_x is the measured pressure, C_0 is pressure offset, C_i are the calibration coefficients, and V_x is the transducer voltage at P_x. All the coefficients from the previous work's calibration, except for C_0, were used to calculate the pressures.

$$P_x = C_0 + C_1(V_x) + C_2(V_x)^2 + C_3(V_x)^3 + C_4(V_x)^4 \qquad \textbf{Eq. 1}^{11}$$

2.3.4 Pitot-Static Probe

To measure dynamic pressure and change in static pressure during taxi testing a pitot-static probe (Figure 2-6) was mounted in the nose of the UAV. The probe was manufactured, calibrated, and tested in-house. Figure 2-7 displays the results of a study conducted on the error in dynamic pressure induced by angle of attack or sideslip. Due to the almost linear section from 0-3°, two regressions were used to fit the data. A linear fit through the origin was used for the first region and a separate 2nd order polynomial fit was selected for the range of angles greater than 3°. The equations of the regression curves for β in degrees are:

$$0\text{-}3^\circ: \quad Error = 0.0033\beta \qquad \textbf{Eq. 2}$$

$$3\text{-}16^\circ: \quad Error = 0.0003\beta^2 - 0.0012\beta + 0.0017 \qquad \textbf{Eq.3}$$

These corrections were later used and will be further discussed in the takeoff and landing analysis.

Figure 2-6: NCSU Pitot-Static Probe

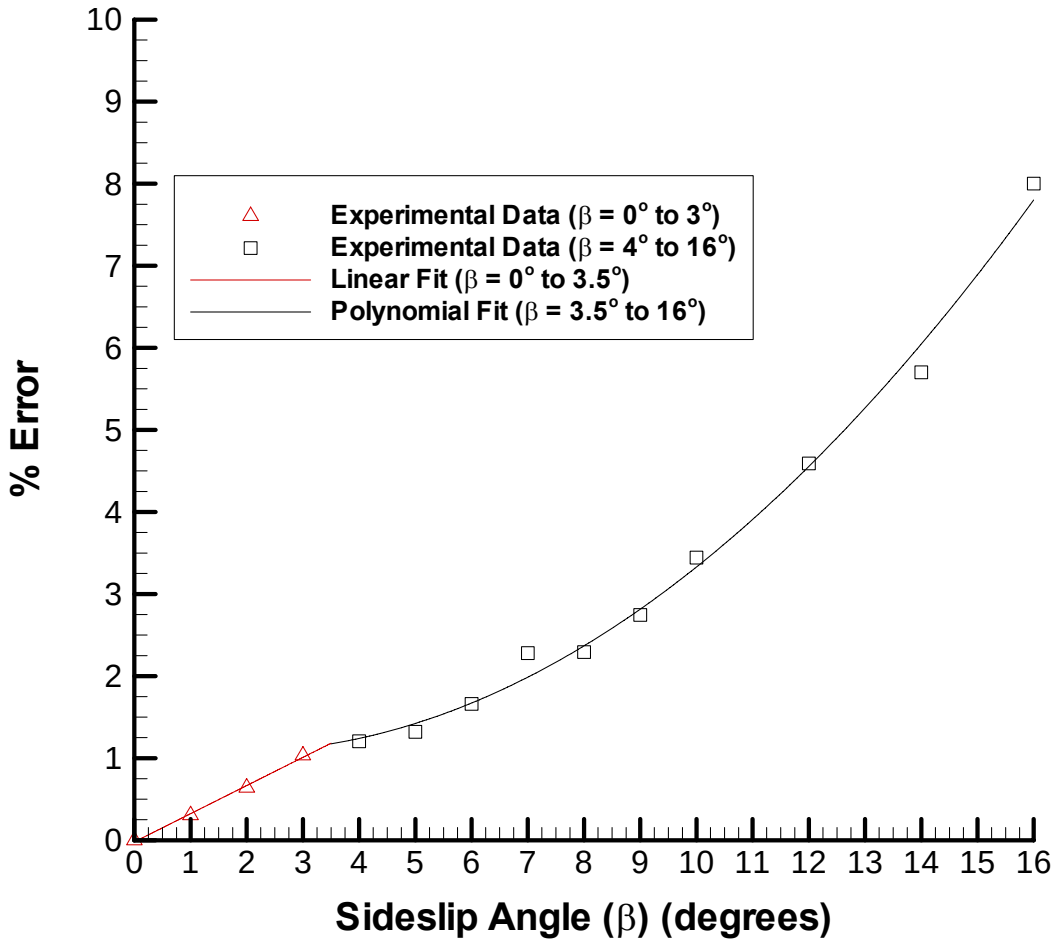

Figure 2-7: Percentage Error on Dynamic Pressure Induced by Sideslip

3 Results and Discussion

Several taxi tests were performed to prepare the UAV for flight testing. Data was collected during all the tests. For taxi testing, the operation of flow control was limited to completely on or off, due to solenoid's capabilities. This work displays the data collected from the taxi test conducted on February 2, 2005. Due to problems encountered throughout the course of taxi testing, this data set proved to be the most complete. Data from other partial data sets was examined under the same methods for comparison. As a result of these comparisons, it was determined the results from the evaluation of the inlet flow distortion and flow control were repeatable and the data from these tests would be sufficient for characterizing the flow distortions and accelerations observed in all the other runs.

Three taxi runs were completed on the test day, two runs at 250 ft and a single run at 375 ft. The runs at 250 ft were conducted with flow control on and off. The single run at 375 ft was with flow control on. The taxi test was terminated prior to the fourth and final run due to an un-commanded aileron throw. The test card detailing the test day weather conditions and events can be found in Appendix C.

In addition to the data sets for each of the runs, data was recorded for static conditions, with and without flow control. This data was used for comparison with the findings of NCSU's previous investigation of inlet flow distortion and flow control effectiveness. The static results also provided a reference point for evaluation of the distortion and flow control in a dynamic setting.

The results of this work are organized in the following fashion. The first section describes the methods for characterizing inlet flow distortion and the effectiveness of the

flow control. Within in this section a short summary of the results from the previous work is provided to establish a basis of comparison for the static runs followed by an evaluation of the distortion and flow control in the dynamic setting. The second section discusses the takeoff and landing performance analysis. The methods for the standard analysis and the reduction of the taxi test data are explained. The section is closed out with the assessment of the takeoff and landing performance using the data measured by the Crossbow VG400 and the NCSU pitot-static probe.

3.1 Inlet Flow Distortion and Flow Control Analysis

There are several methodologies for the qualitative and quantitative analysis of flow distortion at the engine inlet face due to the extreme geometry changes associated with highly compact serpentine inlet ducts. The methodology selected for the investigation of inlet flow distortion and the effectiveness of flow control by the researcher in the previous work was outlined in Society of Automotive Engineers ARP 1420. This methodology has been the standard for parameterization of inlet flow distortion for many years. To maintain continuity with the previous work, the same distortion descriptor elements were used in this work.

To evaluate the inlet flow distortion, steady-state or "time averaged" pressure data across a worst case scenario was used. It was determined in the previous work that the time averaged data, along with other information, would provide sufficient data points to assess inlet flow distortion and the value of the flow control.

One disadvantage of analyzing only the steady-state pressure data across the entire worst case scenario is the effect of aircraft airspeed is lost because a range of velocities is being evaluated. With the flight computer configured to collect data at 50 samples per

second, there is the ability to examine certain inlet flow distortion parameters across smaller ranges and at instances in time for the effects of velocity.

To create a visualization of the distortion at the AIP, percentage of pressure recovery was used. The difference in the analysis of the static and dynamic data is found in this distortion descriptor. Pressure recovery is the ratio of the total pressure measured at the inlet rake plus the atmospheric pressure to the sum of atmospheric pressure and dynamic pressure as shown in Equation 4. For the static settings, the dynamic pressure is zero.

$$\text{Pressure Recovery Ratio} = \frac{\left(p_0 + p_{atm}\right)}{\left(p_{atm} + \bar{q}\right)} \qquad \textbf{Eq. 4}$$

The other distortion parameters are separated into two types, circumferential and radial elements. Circumferential distortion is a description of the distortion as a ring-by-ring basis. Figure 2-7 displays a typical circumferential distortion pattern for a single ring.

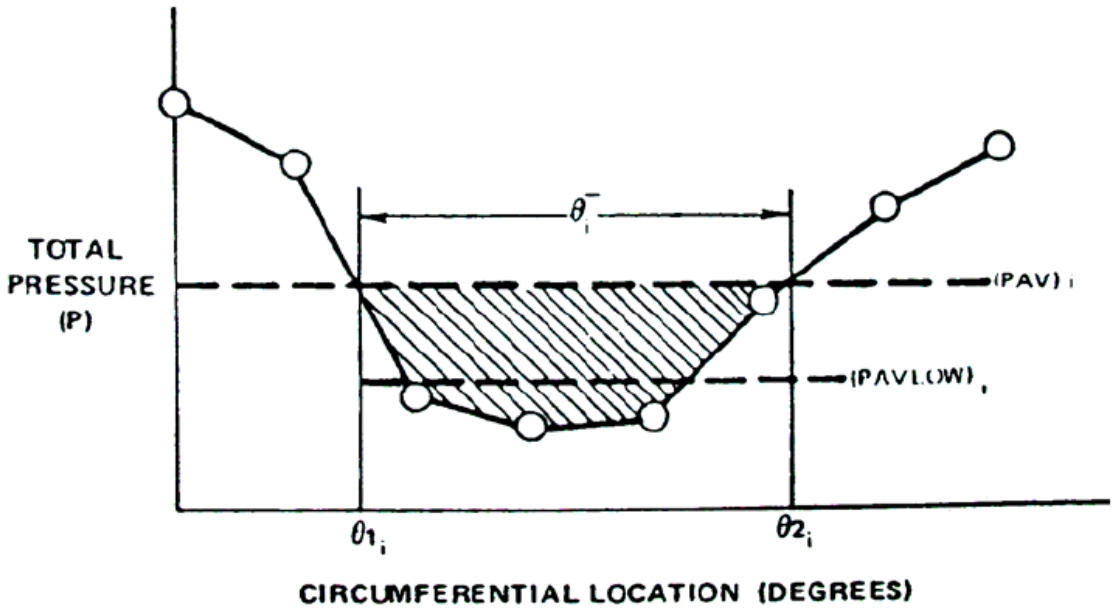

Figure 3-1: Typical Circumferential Distortion Pattern for a Single Ring[10]

Circumferential distortion is broken down further into intensity and extent elements. The circumferential intensity element is a measures the magnitude of the pressure distortion per ring. The equation for calculating the circumferential intensity element is:

$$\left(\frac{\Delta PC}{P}\right)_i = \frac{(PAV)_i - (PAVLOW)_i}{(PAV)_i} \qquad \textbf{Eq. 5}$$

PAV is the average pressure for a single ring. *PAVLOW* is the average of the pressures less than the ring average pressure. Circumferential extent is the angular size of the low pressure region displayed in Figure 2-7. The extent element is defined as:

$$(\theta^-)_i = \theta_{2i} - \theta_{1i} \qquad \textbf{Eq. 6}$$

Radial distortion only has a component of intensity. That element is a measure of the degree of the distortion on each ring to the total engine face. The equation for the radial intensity element of a single ring is, where *PFAV* average total pressure across the engine face:

$$\left(\frac{\Delta PR}{P}\right)_i = \frac{(PFAV) - (PAV)_i}{(PFAV)} \qquad \textbf{Eq. 7}$$

Due to the large amount of pressure data that was collected per taxi run, a MATLAB® script was written to calculate all of these inlet flow distortion descriptors. The code is located in Appendix B-3.

3.1.1 Previous Work Results

The static testing of the propulsion system with flow control designed in the previous work displayed improvements in system performance and engine inlet face distortion when the flow control was implemented. In this investigation, it was determined that the worst case scenario for flow distortion was the full throttle range. Results of the flow distortion analysis and the value of flow control were presented for this range. The use of flow control

reduced the maximum local total pressure loss by 4% and increased the average pressure recovery across the engine inlet face by around 3%. The circumferential distortion extent element was reduced by 22% and the intensity was reduced by about 10% with flow control. Overall there was 42% reduction in engine face distortion. In terms of propulsion system performance the engine experienced a thrust increase of 3% from 107 lbs to 110 lbs and the thrust specific fuel consumption was reduced by 3%. The success of the flow control in reducing the inlet flow distortion translated into propulsion system performance improvements.

3.1.2 Taxi Test Results

There are a few important points to make before discussing the results obtained during the taxi tests. Even though the same propulsion system, that was designed and tested in the previous work, was installed in the test UAV, there was a notable reduction in thrust. Between the static engine testing performed for the earlier work and taxi testing, the AT1500 turbojet engine had to be sent back for a major overhaul, modifications and several hours of engine run time were accrued. These factors contributed to a 30% reduction in thrust. This was reason for the collection of data in the static situation. With the static data, the basic flow properties were verified with those found in the previous work.

Upon examination of the data collected during taxi testing, pressure data from one of the total pressure ports in the inlet rake was not following the expected trends. Visual inspection of the system revealed that the tubing from the port had been clogged. To amend this erroneous data point, the pressures from the ports above and below were averaged. This practice was deemed acceptable by the methodology discussed in ARP 1420.[10]

As discussed in the previous section, the worst case scenario for inlet flow distortion is the full throttle range. All analysis for the inlet flow distortion and implementation of flow control were conducted at this worst case scenario. To determine the range of full throttle, the manifold pressures and throttle commands were examined. It was determined that the manifold pressure response would provide a better indication of the full throttle range because it was directly related to the engine spool-up. There is a delay between the spool-up of the engine compared to pilot's throttle command. Figure 3-2 is an example of throttle command compared to the manifold pressure. The delay in engine spool-up is approximately 6 seconds.

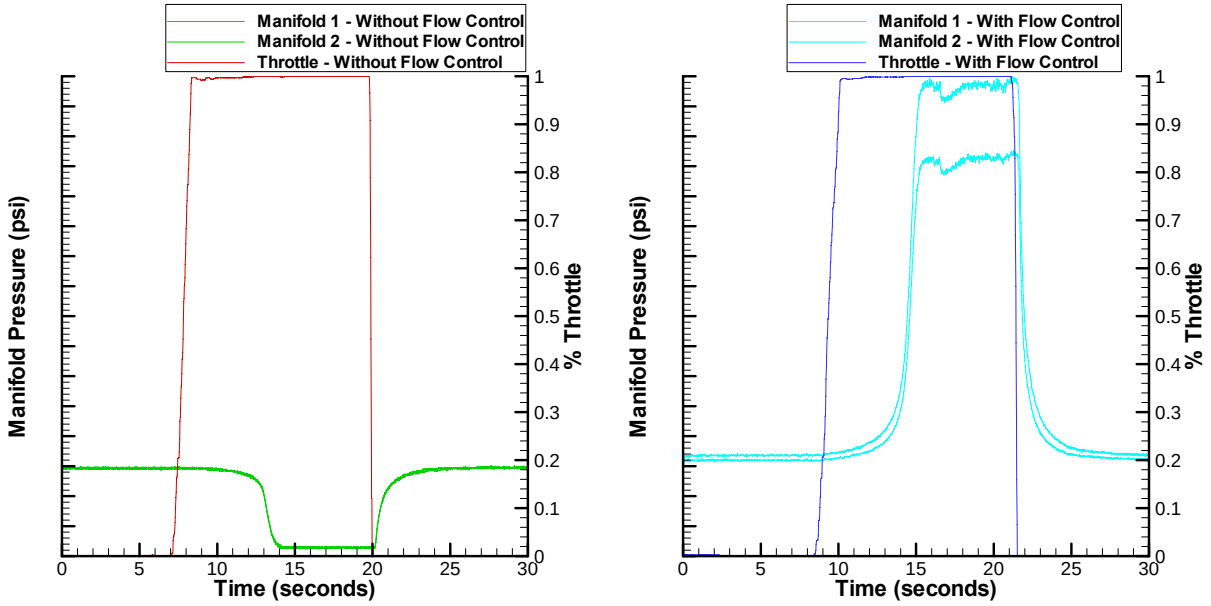

Figure 3-2: Comparison of Throttle Command to Manifold Pressure for Determining Full Throttle Region – With and Without Flow Control

1.1.1.3 Static Runs

Below in Figure 3-3 are the two engine face total pressure scans for flow control on and off at full throttle. The basic distortion patterns match the previous work conducted at NC State. Without flow control implemented there is notable large region of distortion. A

maximum total pressure loss of 30% is seen without flow control with an average pressure recovery of 93%. With flow control engaged it can be noted that the large area of distortion has diminished and propagated along the upper circumference. The maximum total pressure was reduced to 24% and the average pressure recovery for the entire face was increased to 96%. The pressure losses are greater when compared to the previous work but the advantage gained with fluidic flow control is comparable.

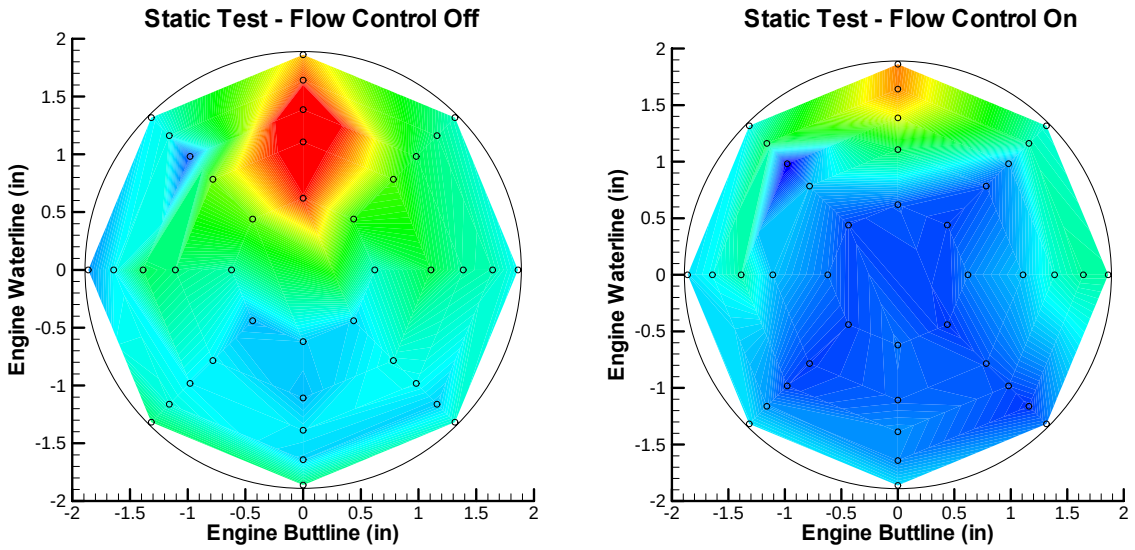

Figure 3-3: Full Throttle Engine Face Total Pressure Distribution With and Without Inlet Fluidic Flow Control – Static Runs

A flow distortion analysis was also conducted on the static runs to determine the circumferential and radial intensity elements. In the Figures 3-4 and 3-5 below, the circumferential distortion for all rings at full throttle can be seen for the flow control on and off cases. Additional plots of ring-by-ring comparisons of the circumferential distortion patterns for the static runs can be found in Appendix D-1.

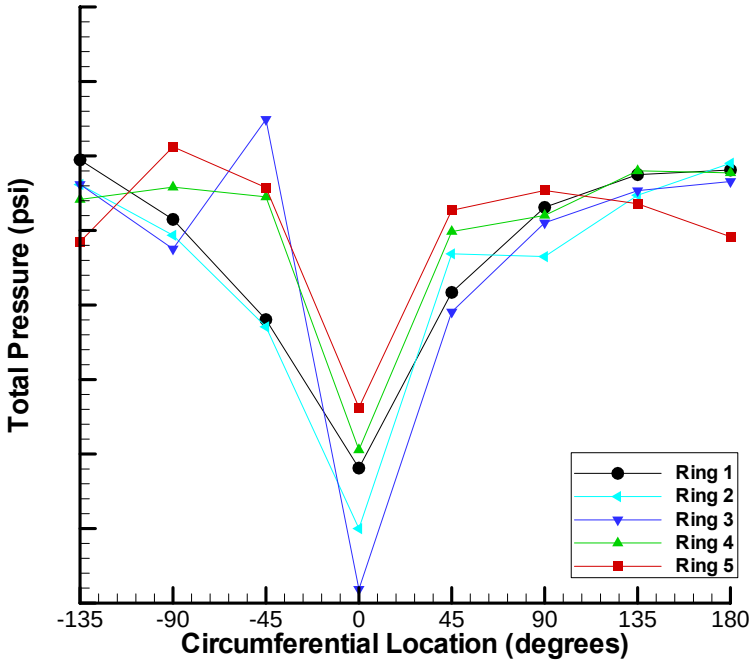

Figure 3-4: Circumferential Distortion Pattern for Each Ring at Full Throttle – Static Run Flow Control Off

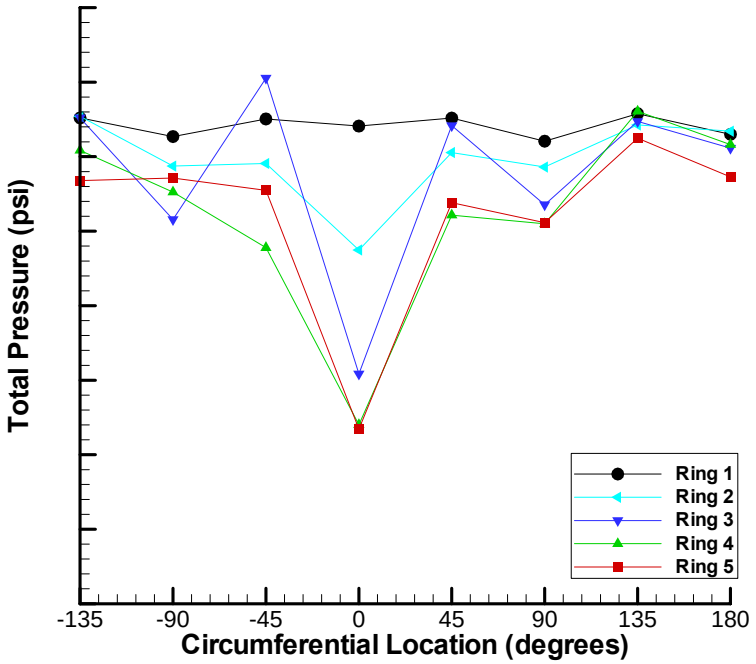

Figure 3-5: Circumferential Distortion Pattern for Each Ring at Full Throttle – Static Run Flow Control On

Table 3-1 compares the time average values of the circumferential intensity element for each ring. With the activation of the flow control the distortion of Ring 1 is reduced by 79%. The average reduction in circumferential intensity for the engine inlet face is approximately 45%.

Table 3-1: Comparison of Ring Circumferential Intensity Elements With and Without Flow Control at Full Throttle – Static Run

Ring	Without Flow Control	With Flow Control
1	0.069	0.014
2	0.072	0.031
3	0.085	0.050
4	0.057	0.051
5	0.045	0.048

Table 3-2 is a comparison of the radial distortion intensity elements for the engine inlet face at full throttle. The radial components of distortion follow the same trend as the previously completed work for the static case.

Table 3-2: Comparison of Ring Radial Intensity Elements With and Without Flow Control at Full Throttle – Static Run

Ring	Without Flow Control	With Flow Control
1	0.003	-0.024
2	0.013	-0.009
3	0.005	-0.002
4	-0.009	0.017
5	-0.009	0.018

The results of the static runs provided a favorable base for comparison with the dynamic runs. The trends observed in the original work done by NC State on the effectiveness of flow control were present in these results.

1.1.1.4 Dynamic Runs

There were three high speed runs during which data was collected, two at a distance of 250 ft and one at 375 ft. Only one run was performed at 375 ft because the taxi test was cut short as discussed earlier. The 250 ft runs will be used for comparison between flow on and off.

In Figure 3-6, a side by side comparison of the engine inlet face total pressure distributions for the 250 feet high speed taxi runs can be seen for an airspeed of approximately 30 ft/s and an angle of sideslip of 3.5°. The flow patterns are consistent with the patterns observed in the static cases. The area of distortion, in red, in the no flow control case is much larger than the static run. The maximum total pressure loss observed in the 250 ft run was 33%, a 10% increase over the static run. The average pressure recovery for the entire engine face is the same as the static run, 93%.

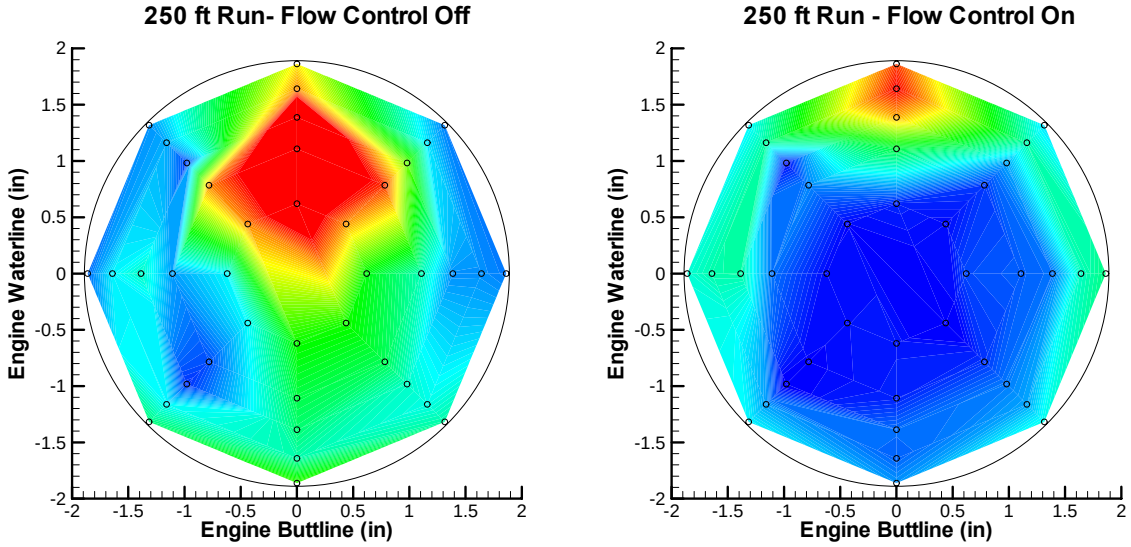

Figure 3-6: Full Throttle Engine Face Total Pressure Distribution With and Without Fluidic Flow Control – 250 ft Runs (Airspeed = 30 ft/s)

With the implementation of fluidic flow control the distortion region is weakened and has moved to the upper circumference as expected. The weakening of the distortion region translates into a reduction of the maximum total pressure loss to 24% with an increase in average pressure recovery of 97%.

As the aircraft's airspeed increased the flow control became more effective. This is evident from examining the full throttle region in the plots of airspeed with the average total pressure recovery across the engine inlet face for the 250 and 375 ft runs with flow control on (Figures 3-7, 8). The average total pressure recovery increases as the dynamic pressure increases. This trend is not present in the runs without flow control. As the aircraft airspeed increases, the average pressure loss at the inlet face increases as shown in Figure 3-9.

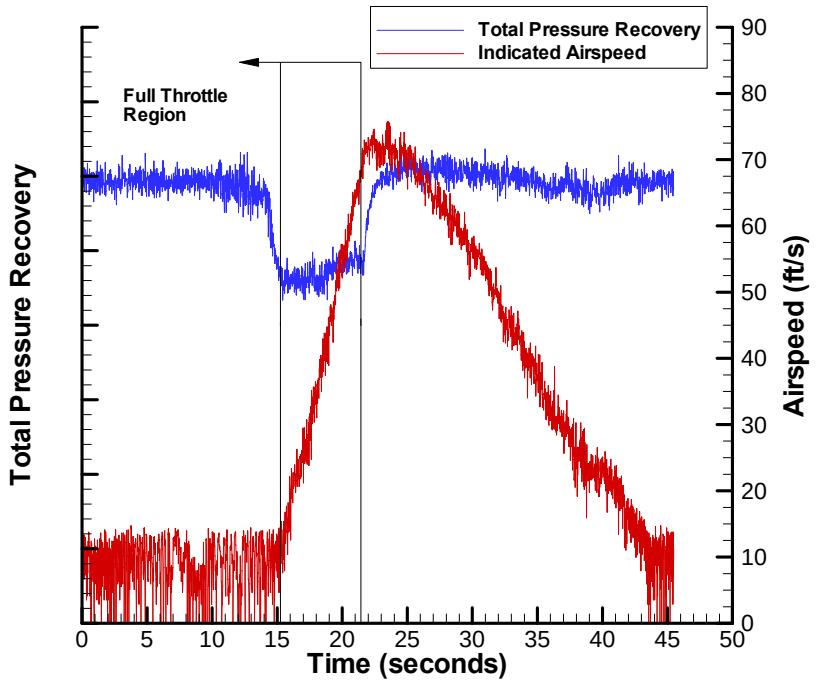

Figure 3-7: Effect of Aircraft Airspeed on the Average Engine Inlet Face Pressure Recovery for the 250 ft with Flow Control

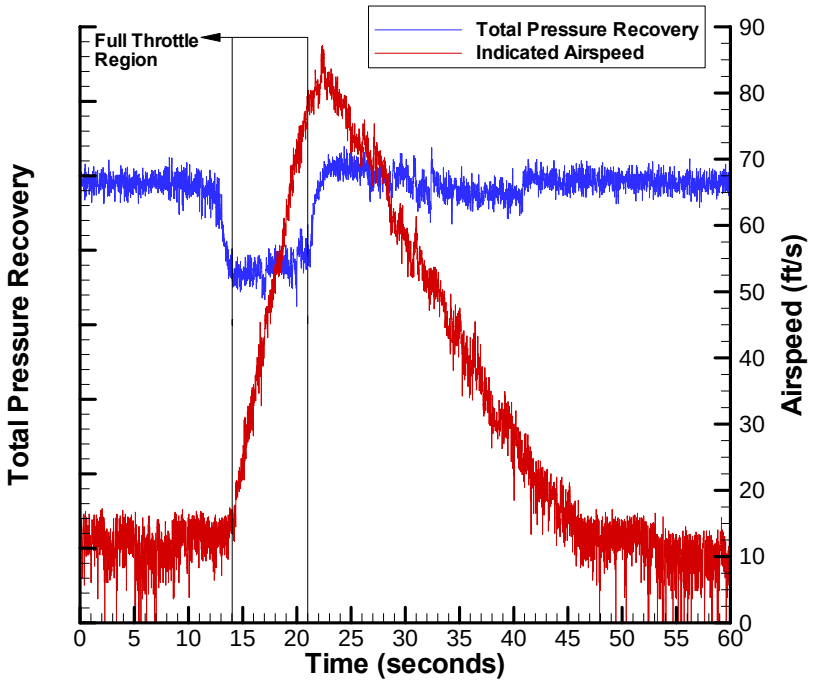

Figure 3-8: Effect of Aircraft Airspeed on the Average Engine Inlet Face Pressure Recovery for the 375 ft with Flow Control

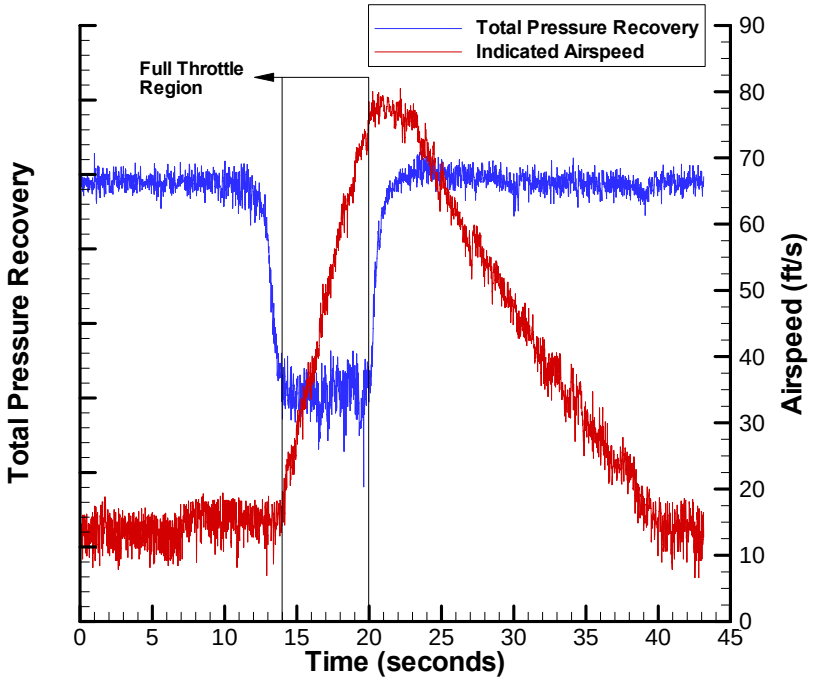

Figure 3-9: Effect of Aircraft Airspeed on the Average Engine Inlet Face Pressure Recovery for the 250 ft without Flow Control

As with the static cases, a flow distortion analysis was conducted. The circumferential distortion patterns for each ring in the inlet rake are shown in Figures 3-10 and 3-11 for both cases. The axes in the plots are to the same scale so the effect of fluidic flow control on the distortion patterns can be identified. The plots show the qualitative effect the flow control has on the inner three rings. With the flow control activated the distortion on those three rings reduced significantly. Additional ring by ring comparisons of the dynamic circumferential distortion patterns can be found in Appendix D-2.

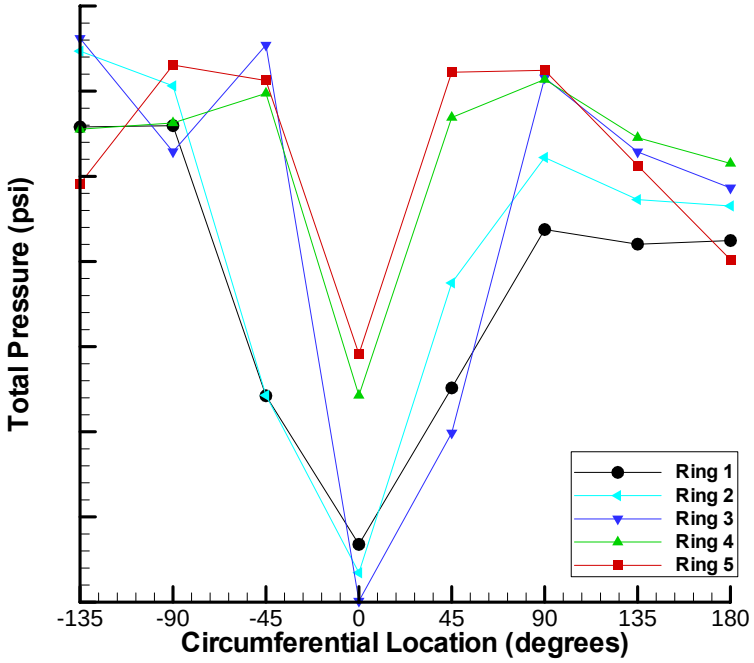

Figure 3-10: Circumferential Distortion Pattern for Each Ring at Full Throttle – 250 ft Run Flow Control Off (Airspeed = 30 ft/s)

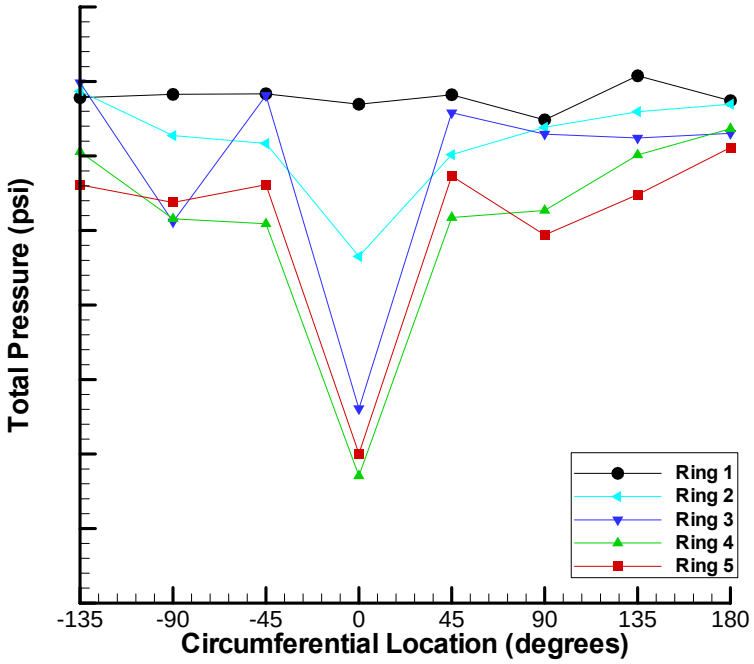

Figure 3-11: Circumferential Distortion Pattern for Each Ring at Full Throttle – 250 ft Run Flow Control On (Airspeed = 30 ft/s)

Table 3-3 displays the time averaged circumferential intensities across the full throttle range. As seen in the static cases the ring with the greatest circumferential distortion is Ring 3. Ring 1 sees the greatest decrease in distortion, nearly 93%. The average reduction in circumferential intensity across the engine face is 40%.

Table 3-3: Comparison of Ring Circumferential Intensity Elements With and Without Flow Control at Full Throttle – 250 ft Runs (Airspeed = 30 ft/s)

Ring	Without Flow Control	With Flow Control
1	0.074	0.005
2	0.084	0.037
3	0.105	0.068
4	0.052	0.059
5	0.049	0.062

Table 3-4 is a comparison of the of the radial intensity elements for the 250 ft runs. The same trends observed in the static runs were found in the dynamic runs.

Table 3-4: Comparison of Ring Radial Intensity Elements with and Without Flow Control at Full Throttle – 250 ft Runs (Airspeed = 30 ft/s)

Ring	Without Flow Control	With Flow Control
1	0.033	-0.034
2	0.014	-0.014
3	0.000	-0.002
4	-0.024	0.025
5	-0.023	0.025

The 375 ft run with flow control on produced similar results to the 250 ft run. The average pressure recovery across the engine face was 97% with a local maximum pressure loss of 22% on the third ring.

3.2 Takeoff and Landing Performance Analysis

3.2.1 Standard Takeoff and Landing Analysis

Prior to taxi testing, an analysis of the UAV's takeoff and landing performance was conducted using standard performance calculations. Approximation equations were used to determine the critical velocities and distances. There are several constants and aircraft parameters needed to solve for takeoff distance using these methods. Table 3-5 lists the necessary parameters for both approaches and the essential equations follow. All of the parameters were calculated or measured except for the rolling coefficient of friction, μ_r, and parasite drag coefficient, C_{Do} with gear down. C_{Do} was an estimate based of wind tunnel data from the aircraft in a clean configuration with assumptions used for drag due to the landing gear. The rolling coefficient of friction is a commonly used estimate for dry, asphalt from

Anderson.[12] The braking coefficient of friction, μ_b, was established experimentally through a "pull test." The value below is for the kinetic state and was determined by measuring the force needed to keep the aircraft rolling with breaks engaged. By dividing the measured force by the weight of aircraft the rolling coefficient of friction due to braking is yielded.

Table 3-5: Aircraft Parameters

Constants	Symbols	Value
Sea Level Density	ρ_∞	0.002376 slug/ft^3
Acceleration Due to Gravity	g	32.2 ft/s^2
Aircraft Parameters		
Weight	W	214 lbs
Wing Reference Area	S	36.4 ft^2
Wing span	b	8 ft
Aspect Ratio	AR	1.76
Aerodynamic Parameters		
Lift Coefficient at α=0°	C_{Lo}	0.03
Max. Lift Coefficient	C_{Lmax}	0.75
Parasite Drag Coefficient (Gear Down)	C_{Do}	0.031
Oswald Efficiency Factor	e	0.77
Engine Parameters		
Maximum Thrust	T	72 lbs
Idle Thrust	T_i	2.8 lbs
Gear Parameters		
Rolling Coefficient of Friction	μ_r	0.02
Braking Coefficient of Friction	μ_b	0.19

$$\textit{Total Drag Coefficient:}\quad C_D = C_{Do} + \frac{C_L^2}{\pi e AR} \qquad \textbf{Eq. 8}$$

$$\textit{Drag:}\quad D = \frac{1}{2}\rho_\infty V_\infty^2 S C_D \qquad \textbf{Eq. 9}$$

$$\textit{Lift:}\quad L = \frac{1}{2}\rho_\infty V_\infty^2 S C_L \qquad \textbf{Eq. 10}$$

$$\textit{Acceleration:}\quad a_x = \frac{g}{W}\left[T - D - \mu_r\left(W - L\right)\right] \qquad \textbf{Eq. 11}$$

$$\textit{Stall Velocity: } V_{stall} = \sqrt{\frac{2W}{\rho_\infty S C_{L\max}}} \qquad \textbf{Eq. 12}$$

The standard safety margin used for liftoff velocity, V_{LO}, is 20% greater than stall, and 30% greater for touch down velocity, V_{TD}. Using these velocities and the approximation equations from Anderson[12], the calculated distances for takeoff and landing are displayed in Table 3-6.

$$V_{LO} = 1.2 V_{stall} \qquad \textbf{Eq. 13}$$

$$V_{TD} = 1.3 V_{stall} \qquad \textbf{Eq. 14}$$

$$s_{LO} = \frac{\left(V_{LO}{}^2\right)\left(W/g\right)}{2\left\{T - \left[D + \mu_r\left(W - L\right)\right]_{0.7V_{LO}}\right\}} \qquad \textbf{Eq. 15}$$

$$s_L = \frac{\left(V_{TD}{}^2\right)\left(W/g\right)}{2\left\{\left[D + \mu_b\left(W - L\right)\right]_{0.7V_{LO}} - T_i\right\}} \qquad \textbf{Eq. 16}$$

Table 3-6: Takeoff and Landing Values from Approximations

	Velocity (ft/s)	Distance (ft)
Takeoff	97.4	515
Landing	105.5	861

Several assumptions were made for the distance equation, including constant thrust and acceleration force evaluated at an instantaneous velocity of $0.7V_{LO}$. The distance equation is later used with velocities from the Crossbow IMU for comparison with the distances calculated from the test data.

3.2.2 Analysis of Experimental Data

Data from these runs was examined to obtain the test aircraft takeoff performance. Two transducers provided the measurements needed to determine these parameters experimentally. The dynamic pressure reading from the pitot-static probe and the X-acceleration from the VG400 were used to develop velocity profiles for evaluating takeoff distances.

Before the data could be analyzed, corrections were necessary to eliminate errors in the transducer measurements attributed to uncontrollable factors of the test day. One of the issues was wind. If the aircraft's path is not in line with the wind heading there is an error in the pitot-static measurements. For this testing, angle of sideslip (β) was the concern. The equations for percent error due to angle of sideslip were included in the previous Pitot-Static Probe section. These were used to eliminate the error in the measurements of dynamic pressure.

Upon extraction of the error due to sideslip, the headwind component was addressed. The following measures were taken to deal with this problem. During taxi testing, weather was monitored from the Automated Weather Observing System (AWOS) at the airport. The reported winds are not instantaneous. The following assumptions were used. It was determined that it would be acceptable to maintain the direction of the winds in the reported weather throughout the entire set of taxi runs. To determine the magnitude of the winds (V_{wind}) for each run, the first ten seconds of dynamic pressure readings when the aircraft was stationary were averaged.

The initial sideslip angle (β_1) for the runs was assumed to be the difference between the wind direction and the runway heading. Using the sideslip angle and the associated

percent error, the dynamic pressure was corrected and the wind magnitude was recalculated. Using the corrected wind velocity and sideslip angle, the headwind ($V_{x,wind}$) and crosswind ($V_{y,wind}$) components were calculated using trigonometric relations. These components were assumed to be constant over the duration of a single run.

With the crosswind component and the measured velocity, the sideslip angle for each data point was recalculated. The appropriate correction was then applied to the dynamic pressure and the new velocities were calculated. Using the corrected velocities and sideslip angle, the indicated airspeed (V_{ind}) was calculated. To obtain the aircraft's indicated ground speed the headwind component was subtracted from the indicated airspeed. A diagram of the velocities and angles can be seen in Figure 3-12.

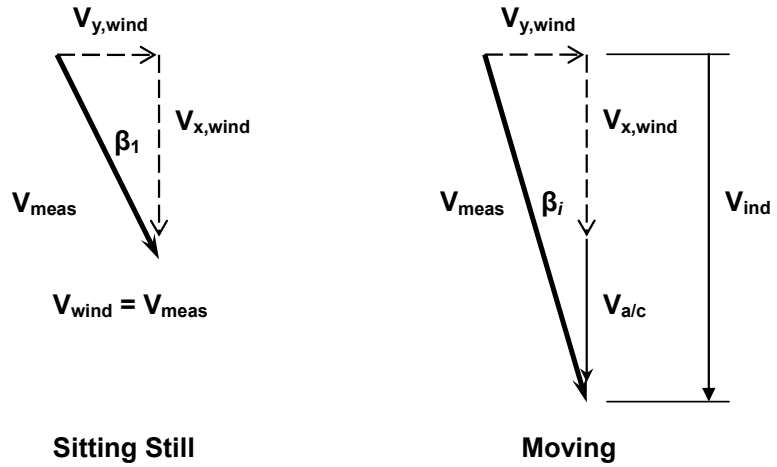

Figure 3-12: Effect of Wind on the Velocity Read by Pitot-Static Probe

On the test day there was 7 knot wind from 40° east of north. This resulted in an initial sideslip angle of 10° off the runway heading. Using the method described above, the comparisons below between the velocity profiles of indicated air and ground speed were developed (Figures 3-13, 14, 15). As explained the offset was due to the headwind present that day.

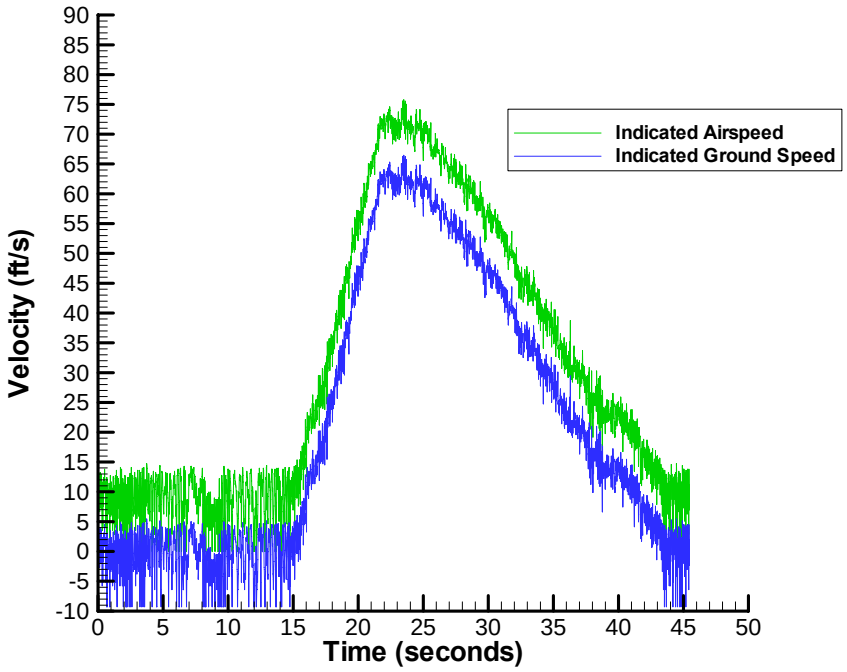

Figure 3-13: Comparison of Indicated Air and Ground Speed for the 250 ft Run Flow Control On

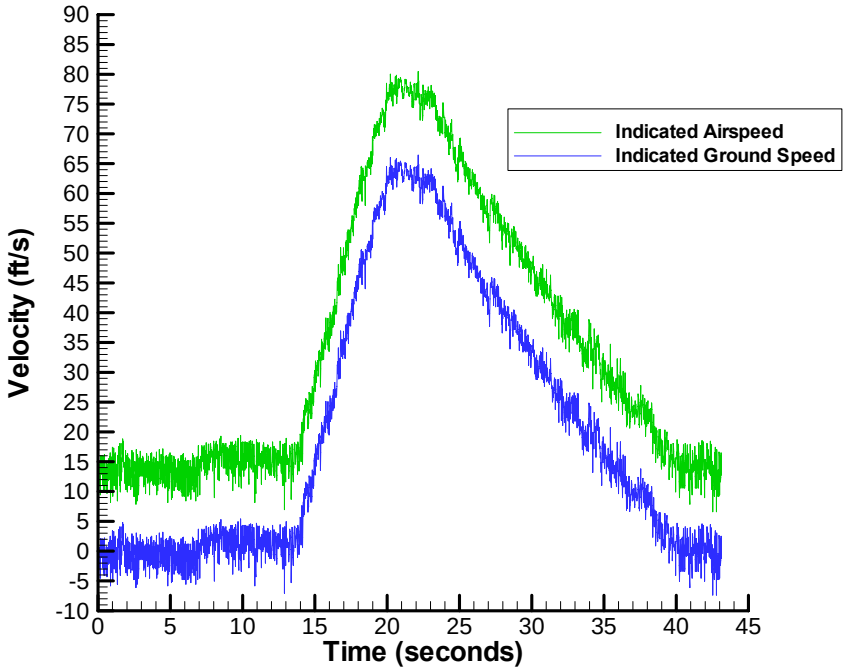

Figure 3-14: Comparison of Indicated Air and Ground Speed for the 250 ft Run Flow Control Off

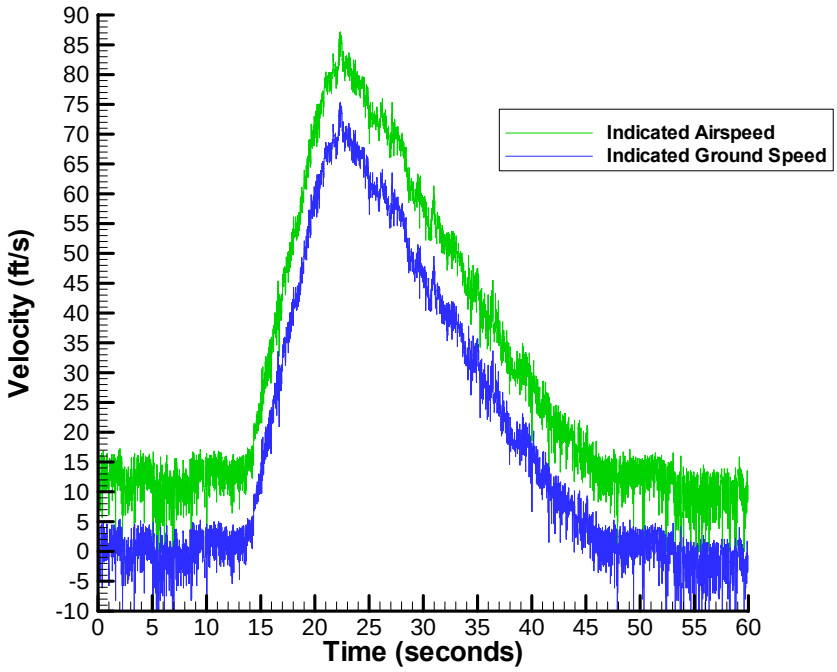

Figure 3-15: Comparison of Indicated Air and Ground Speed for the 375 ft Run Flow Control On

The accelerations measured by the VG400 were used to verify the velocities calculated from the dynamic pressures read by the pitot-static tube. Using accelerations in the X-direction and a simple Euler numerical integration scheme, the velocities and distances traveled during each run were calculated. The following equation was used for integrating the velocities (Equation 17). A similar equation was used for integrating the velocities to obtain the distances.

$$v_i = a_i \cdot \Delta t + v_{i-1} \qquad \textbf{Eq. 17}$$

Figures 3-16, 3-17, and 3-18 are plots of the acceleration in the *x*-direction with integrated velocity and distance profiles.

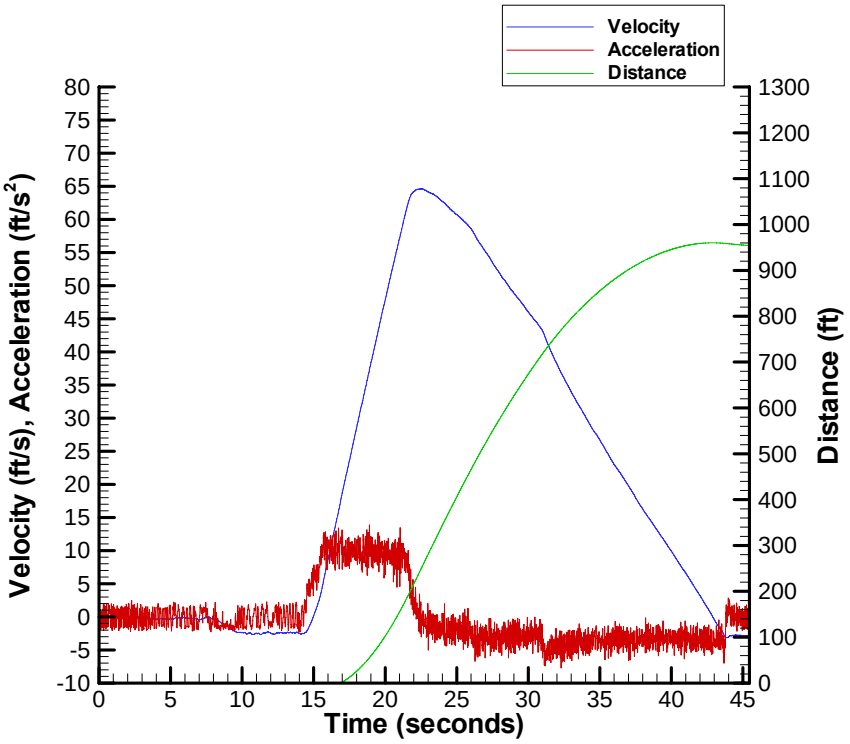

Figure 3-16: Accelerations, Velocities and Distances from the Crossbow IMU for the 250 ft Run Flow Control On

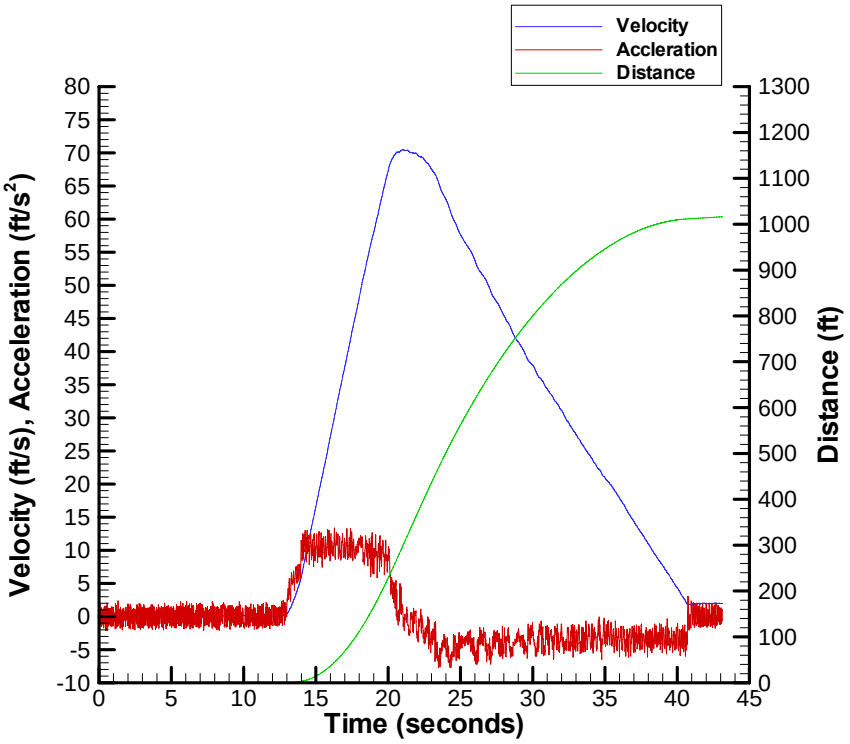

Figure 3-17: Accelerations, Velocities and Distances from the Crossbow IMU for the 250 ft Run Flow Control Off

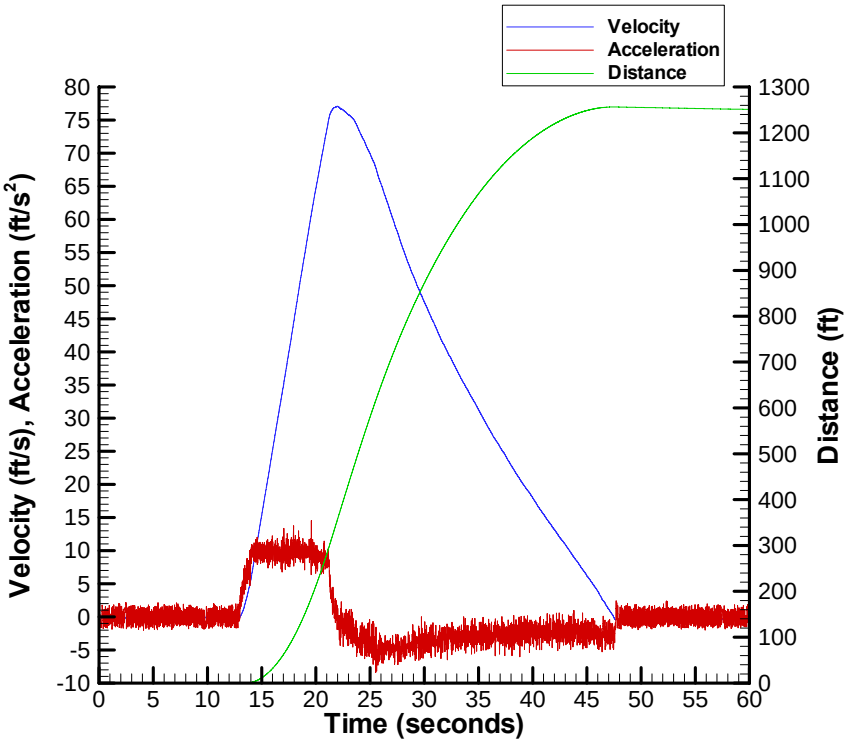

Figure 3-18: Accelerations, Velocities and Distances from the Crossbow IMU for the 375 ft Run Flow Control On

Figures 3-19, 20, and 21 are comparisons of the overall velocity profiles from both instruments. As expected the profiles from the dynamic pressure readings and the Crossbow accelerations are very similar. The differences in the profiles can be attributed to the assumptions made for constant wind and direction during the data reduction.

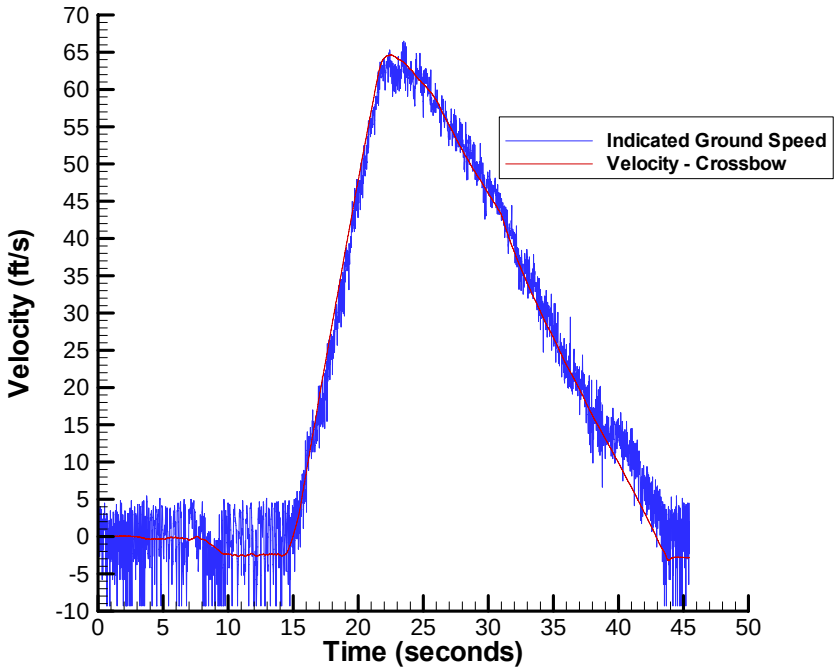

Figure 3-19: Comparison of Velocity Profiles from Crossbow and the Pitot-Static Probe - 250 ft Run Flow Control On

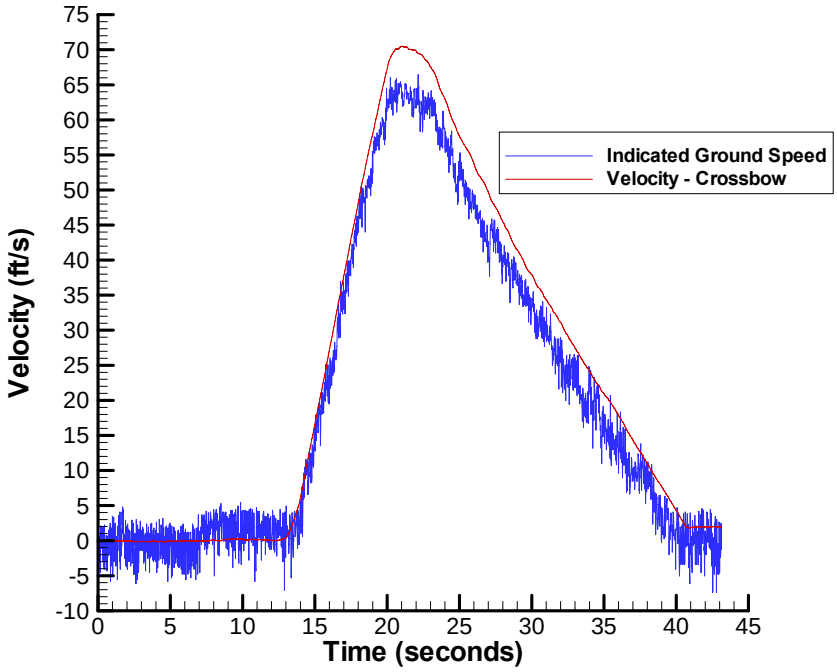

Figure 3-20: Comparison of Velocity Profiles from Crossbow and the Pitot-Static Probe - 250 ft Run Flow Control Off

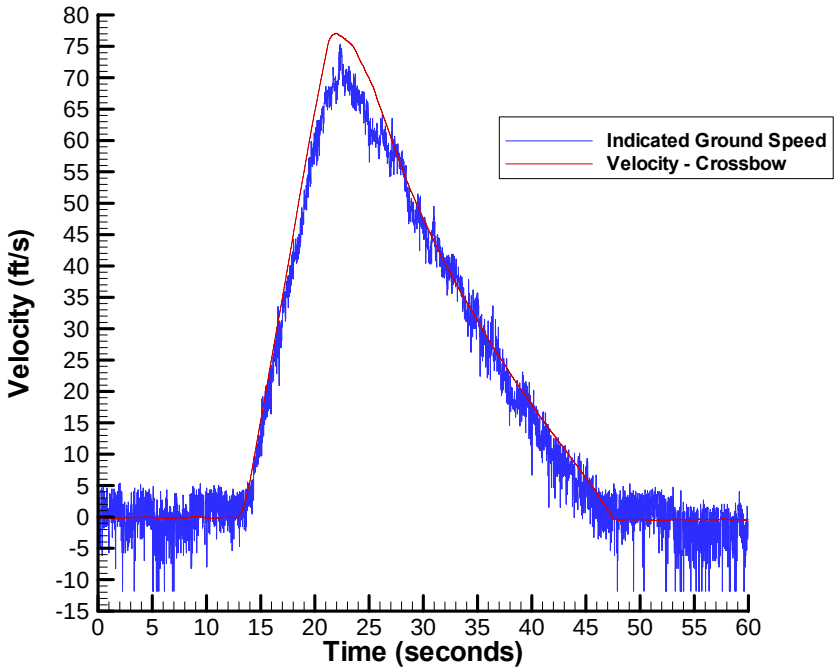

Figure 3-21: Comparison of Velocity Profiles from Crossbow and the Pitot-Static Probe - 375 ft Run Flow Control On

From inspection of the plots of the Crossbow accelerations and velocities, a slight reduction in the acceleration was observed as the velocity increased. This is due to the fact that drag increases with the airspeed while the other contributions to the acceleration are relatively constant. These areas will be discussed in depth later. Also in the deceleration region of the 250 ft run with flow control on, a jump in the measurement is present because the brakes were eased in initially then fully engaged at that point.

To examine the takeoff performance of the aircraft, focus will be placed on the 250 ft run with flow control. This was the first run of the test and it is the closest situation to actual preparation for a takeoff for flight. The change in weight due to fuel burn between the engine start and lining up on the run for the run would be similar to flight operations. A clear record

of times for interpolating weights throughout the taxi test was not kept; therefore the weight will be kept constant for analysis 214 lbs.

To obtain the accelerations in the X-direction for the run, a 2nd order polynomial fit was applied to the full throttle region of the 250 ft run to effectively filter out the noise in the measurement (Figure 3-22). After shifting the equation for the quadratic fit to time zero, the accelerations and net forces were calculated for a range of time. Lift and drag values were calculated from velocities obtained from integrating the velocities across the time range and were adjusted for the headwind that was present during the run. For simplicity the headwind was kept constant across the whole run as previously assumed when correcting airspeed to ground speed.

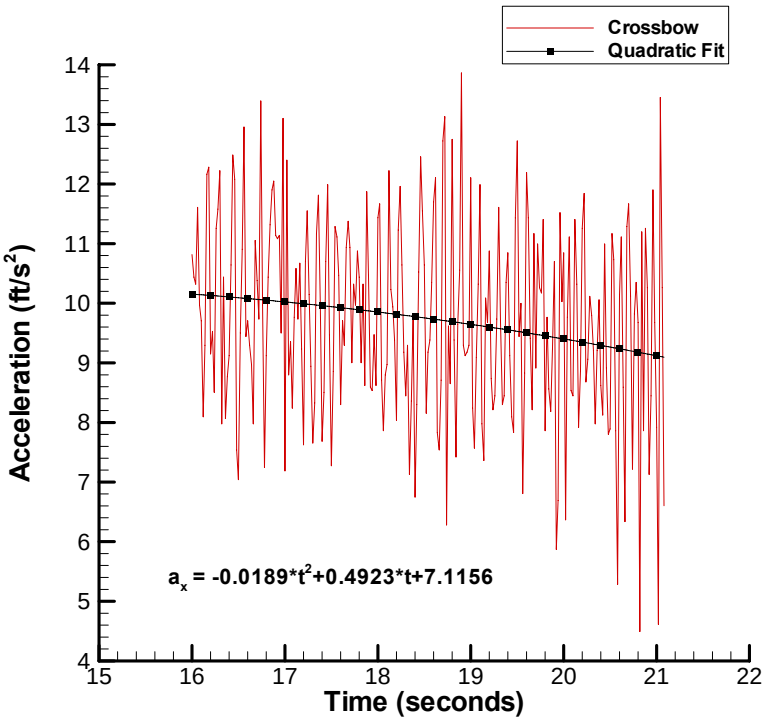

Figure 3-22: Measured Accelerations in X-direction from Crossbow IMU and Quadratic Fit for Filtering Measurement Noise

Assuming the initial value of the net force to be the thrust of the aircraft and less rolling friction constant across the length of the run, the calculated drag, including the headwind, was subtracted and divided by the mass of the aircraft to achieve predicted accelerations. Figure 3-23 shows the comparison of the accelerations extrapolated to the takeoff velocity.

Examining the comparison of the predicted and measured values shows that the aircraft is performing below expectations. This can be attributed to a combination of greater drag than predicted and a reduction of thrust due to increase in velocity. There is no instrumentation on board to measure the thrust or the drag the aircraft is producing across a run to separate the contributions of each. This realization of this trend is important to note for future flight performance.

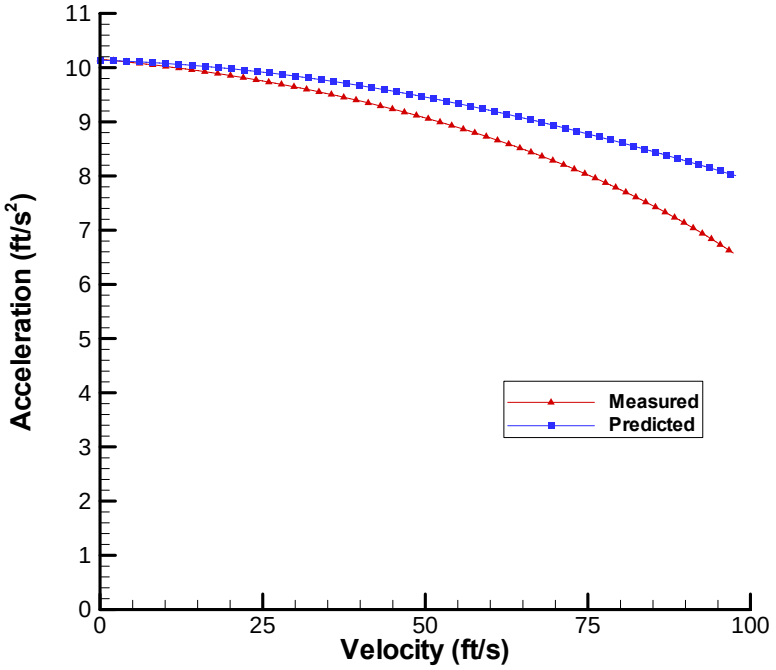

Figure 3-23: Comparison of Acceleration Profile with Removal of Drag and Rolling Friction Force Due to Lift

Using the quadratic equation from the measured a_x, a takeoff distance was extrapolated for the takeoff velocity of 97.4 ft/s. A s_{LO} of 572 ft was obtained from the integrations. This value is slightly longer than the 525 ft takeoff distance obtained from integrating the velocities from the predicted accelerations. Figure 3-23 displays the takeoff velocity profiles for both predicted and measured performance.

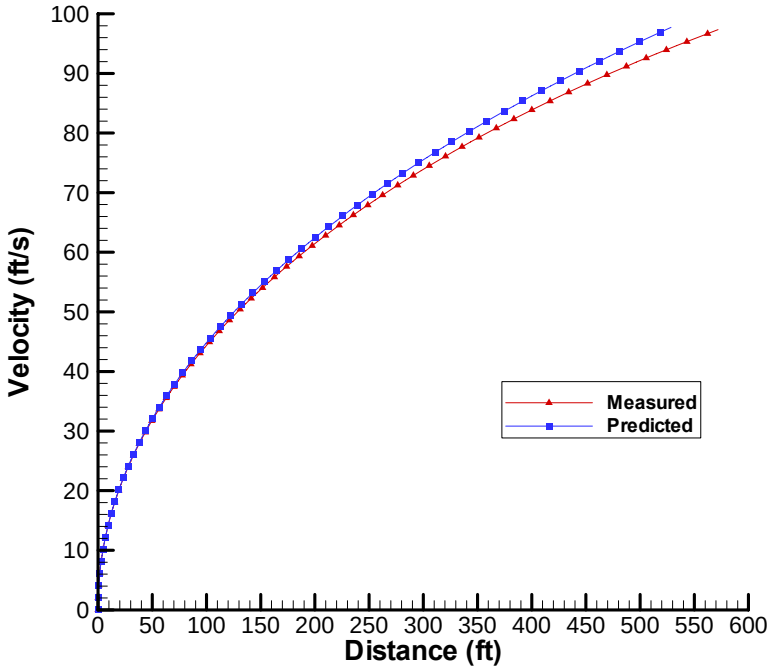

Figure 3-24: Takeoff Velocity Profiles for Predicted and Measured Performance (V_{LO} = 97.4 ft/s, Weight = 214 lbs)

In each of the runs the distance for the vehicle to stop is longer than expected. Using the approximation equations from the previous section and the maximum velocities from each run, the measured and calculated distance values were compared. The distances and maximum velocities are in Table 3-7. The fully fueled weight was used as a worst case

scenario for the approximation equations. Even with that consideration, the measured distances exceed the approximations by a significant amount.

Table 3-7: Approximation and Measured Values for Stopping Distances

Run	Velocity (ft/s)	Distance (ft)	
		Measured	Calculated
250 ft – Flow On	65	757	327
250 ft – Flow Off	71	775	390
375 ft - Flow On	77	966	459

One possible reason for this issue could be the overestimation of the braking coefficient of friction, μ_b. Sources of error in the test that may have contributed to the incorrect value include human error, calibration and hysteresis of the scale, or effects of higher speed.

Using the deceleration region and a linear regression, an estimated landing distance was calculated. The distance was integrated by starting with the touch down velocity, 105.5 ft/s, and decreasing incrementally until a final velocity of 0 ft/s was reached. The landing distance for the aircraft was calculated to be around 1663 ft. This distance is much longer than the distance of 861 ft obtained from the approximation equation. These landing distances were examined at the fully fueled aircraft weight, 214 lbs as a worst case scenario. For a standard flight and landing situations, the approximation equations were evaluated and the measured accelerations were scaled with a weight of 178 lbs assuming a 25% fuel reserve. The landing value from the approximation was 851 ft and the measured distance was 1300 ft. Fortunately, the Harnett County Airport can accommodate a landing distance of this magnitude.

3.3 Summary of Results

The taxi testing of the test UAV provided useful data for the analysis of inlet flow distortion, the value of the flow control, and the determination of important takeoff parameters. The static data provided a basis of comparison for the dynamic cases and a verification of the basic flow characteristics observed in past works conducted by NCSU in fluidic flow control. The static cases exhibited a 3% increase in average total pressure recovery across the engine face and a significant reduction in the local maximum pressure losses. The dynamic case of flow control off displayed a larger area of distortion as expected but maintained similar average total pressure recoveries across the engine face. The implementation of the fluidic flow control reduced the average total pressure recovery by 4%. Also as the velocity increased the flow control became more effective.

The accelerations collected by the Crossbow VG400 and collected dynamic pressures provided the necessary data to for analyzing takeoff and landing performance. Examination of the accelerations yielded important trends about the effect of velocity on thrust and the drag of the aircraft. A combination of more drag than expected and possible thrust losses due to the increase velocity are attributed to the lower than predicted takeoff performance. Landing and takeoff distances were found using the approximation equations and calculations from the measured data. The measured takeoff distance was about 10% longer than predicted, while the error in landing distances was much larger due to an overestimation of the braking coefficient of friction. Table 3-8 is a summary of the landing and takeoff distances.

Table 3-8: Comparison of Theoretical for Analyzing Takeoff and Landing Distances

Method	Takeoff Distance (ft)	Landing Distance (ft)	
		W = 214 lbs	W = 178 lbs
Predicted	525	861	851
Experimental	572	1663	1300

4 Conclusions

This project continued the previous work conducted at NC State University in the field of fluidic flow control in a highly serpentine inlet duct. The same propulsion system designed and statically tested in the earlier work was installed in a test UAV for evaluation of the flow control and inlet engine face distortion near flight operating speeds. The taxi testing also allowed for the takeoff performance to be analyzed.

Without flow control, the distortion characterized by a low pressure regions in the inlet engine face were enlarged during the dynamic runs. An average pressure recovery across the entire engine inlet face of 93% was observed with maximum local pressure losses of 33% in the third ring of the inlet rake. The local maximum pressure losses were much larger than the observed losses in the static analysis, ranging from 2% to 8% depending on the ring. The circumferential distortion patterns were similar to the patterns in the static analysis except for the slightly larger distortion.

When the flow control was initiated the results were similar to those observed during the static cases. With flow control the total pressure recovery across the whole face was increased by 4% to 97%. The maximum local pressure loss was reduced by 10%. Also noted was the fact that as the aircraft's airspeed increased the flow control system became more effective.

The analysis of the UAV's takeoff and landing performance provided useful information for future flight testing operations. With takeoff and landing distances calculated, important conclusions were drawn. Upon examination of the acceleration regions of the taxi runs, it was determined that due to greater drag than expected and possible thrust

losses due to velocity the aircraft performs below predictions. An difference of 10% was observed between takeoff distances calculated fro the measured and predicted accelerations. The landing analysis led to the conclusion that the braking coefficient of friction was overestimated. Before future flight testing, this parameter needs to be investigated to determine a better estimate for quick calculations.

This work covered the taxi testing of a UAV with an installed propulsion system with flow control in a highly compact serpentine inlet duct. Results further verified the extent of the engine inlet distortion and the value of the flow control for static cases and expanded the research into dynamic settings. The takeoff and landing analysis provided insight into the aircraft's performance. Further flight testing would allow the further expansion of the evaluation of the flow control system for higher speeds and other design cases.

5 References

1. Kumar, R., "Tactical Reconnaissance: UAVs versus Manned Aircraft," *AU/ACSC/0349/97-03*, March 1997.

2. Nichols, M., "Uninhabited Combat Air Vehicles and Commercial Satellites: 'The Missing Link'," *AU/AWC/RWP/188/1998-04*, April 1998.

3. Rabe, A.C., "Serpentine Inlet Duct Flow Control Scheme at Designand Off-Design Simulated Flight Conditions." *PhD Dissertation*, Department of Mechanical Engineering, Virginia Tech, Blacksburg, VA, 2003.

4. Hamstra, J.W., Miller, D.N., Truax, P.P., Anderson, B.H. and Wendt, B.J., "Active Inlet Flow Control Technology Demonstration," *ICAS Paper 2000-6.11.2*, August 2000.

5. Collie, W.V., "Design and Analysis of an Unmanned Aerial Vehicle Propulsion System with the Fluidic Flow Control Inside a Highly Compact Serpentine Inlet Duct," *MS Thesis*, Department of Mechanical and Aerospace Engineering, NC State University, Raleigh, NC, 2003.

6. Beamon, D.A., "Propulsion System Design and Testing for a Remotely Piloted Vehicle Powered by a Mini-Turbojet Engine," *MS Thesis*, Department of Mechanical and Aerospace Engineering, NC State University, Raleigh, NC, 2000.

7. Heinzen, S.N., "In-Flight Application of Active Seperation Control Using Pulsed Jet Blowing," *MS Thesis*, Department of Mechanical and Aerospace Engineering, NC State University, Raleigh, NC, 2000.

8. Hall, C.E., "A Real-Time Linux Based System for Flight Testing of Remotely Piloted Vehicles," Proc. IEEE 19th Digital Avionics System Conference, October 2000.

9. *VG400 Series User's Manual*, Revision A, Document 7430-0002-03, Crossbow Technology, Inc., San Jose, California, June 2005.

10. ARP 1420: Gas Turbine Engine Inlet Flow Distortion Guidelines, *Society of Automotive Engineers, Inc.,* March 1978.

11. *ESP-Miniature Pressure Scanners User's Manual*, Pressure Systems, Inc., Hampton, Virginia, August 1999.

12. Anderson, J.D., *Introduction to Flight, Fourth Edition*, McGraw Hill, Boston, 2000, pp. 424-429.

APPENDICES

Appendix A: Taxi Test Plan

UAV
Taxi Test Plan
Flight Research
North Carolina State University, Raleigh, NC

I. Purpose. To establish the procedure for the test vehicle low and high speed taxi tests to be conducted at the Harnett County Airport (KHRJ), Erwin, NC.

II. Objectives. To validate the ground handling, under power, of the research vehicle. This includes steering and braking operations. In addition, the high speed taxi test is to verify and/or update the takeoff performance of the UAV. A secondary objective is to obtain data about the inlet performance with and without the flow control system in use in a dynamic situation.

III. Vehicle Configuration. The UAV will be configured for flight.

IV. Avionics Configuration. The avionics will be in the flight configuration. The onboard flight computer system, LIFT System, will be used to collect data from the instrumentation array. The instrumentation array is given in the following table. The transducers that provide information to the takeoff performance are required for the high speed taxi test.

Transducer	***Quantity***	***Go/No-Go Status***
Crossbow IMU	Angular rates: P,Q,R	Required
	Acceleration: A_x, A_y, A_z	Required
NCSU Pitot-Static Probe	Pitot, Static	Required
	AOA, AOS	
PSI ESP-64 Module	Inlet flow, ARP 1420	
Tao Systems, CVA 12 channels	Inlet Surface Flow Measurements	
Preseure XD	Manifold Pressure	
AMT 1500 ECU	EGT, RPM	Required
A/C Transmitter and Receiver	Pilot Link	Required

1) Weather Limits.

I **Winds.** 12 kt maximum sustained wind with gusts less than 5kt. The crosswind component cannot exceed 8kt.

II **Visibility.** Greater than 3sm.

III **Precipitation.** None. Surface must be dry.

2) Low Speed Taxi Test.

I **Location.** Open area of apron and taxiway.

II **Required Personnel.** The Flight Crew and Support Team, except the Pilot, will be required.

III **Procedure.**

a. **Engine Start Position.** The Engine Start Checklist will be completed in a corner of the apron.

b. **Safety Guards.** During the taxi operations on the apron, Safety Guards will remain on the outside of the path to restrain UAV if directed.

c. **Problems.** Any problems that are encountered, the test will be placed on hold. If adjustments can be performed via the transmitter, they will be made and the test continued. If mechanical adjustments are required, the engine will be shutdown for the modifications that are needed.

d. **Low Speed Taxi Card.**

1. Taxi away from the start position.
2. Test brakes.
3. Proceed at speeds less than 8kts.
4. Left and right turns at various dual rate settings for the rudder.
5. Braking as required.
6. Proceed to taxiway.
7. Accelerate, not to exceed 13kts, in a straight taxi.
8. Decelerate and turn around, repeat.
9. Return to the start position.

e. **Complete the Shutdown Checklist.**

IV **Risk.** Risk during the low speed taxi test is minimal.

3) High Speed Taxi Test.

I **Location.** Runway 05 or 23 as determined by the wind.

II **Required Personnel.** The Flight Crew and Support Team.

III **Procedure.**

a. **Engine Start Position.** The Engine Start Checklist will be completed as for a flight.

b. **Aircraft Handler.** An Aircraft handler will remain at the Start Position. During the taxi back to the start position, the Aircraft Handler will provide hand and arm signals to the Flight Crew to position the UAV in the high speed taxi start position.

c. **Runway Markings.** Markings will be made on the edge of the runway at 250 and 375 feet from the start position. These will be the position of the Flight Crew during the high speed taxi runs. Note: for high winds distances may be reduced to prevent unintentional flight.

d. **Problems.** If any problems are encountered the test will be placed on hold. If adjustments can be performed via the transmitter, they will be made and the test continued. If mechanical adjustments are required, the engine will be shutdown for the modifications that are needed.

e. **High Speed Taxi Card.**

1. Taxi away to the high speed taxi start position.
2. Lock brakes.
3. Flight Crew moves to the 250 foot position.
4. Inlet flow control-ON.
5. Apply full power and release brakes.
6. Reduce thrust to idle as the aircraft passes the Flight Crew.
7. Brake as needed.
8. Inlet flow control-OFF.
9. Taxi back to high speed taxi start position.

1. Lock brakes.
2. Apply full power and release brakes.
3. Reduce thrust to idle as the aircraft passes the Flight Crew.
4. Brake as needed.

5. Taxi back to high speed taxi start position.

1. Lock brakes.
2. Flight Crew moves to the 375 foot position.
3. Inlet flow control-ON.
4. Apply full power and release brakes.
5. Reduce thrust to idle as the aircraft passes the Flight Crew.
6. Brake as needed.
7. Inlet flow control-OFF.
8. Taxi back to high speed taxi start position.

1. Lock brakes.
2. Apply full power and release brakes.
3. Reduce thrust to idle as the aircraft passes the Flight Crew.
4. Brake as needed.
5. Taxi back to high speed taxi start position.

IV Complete the Shutdown Checklist.

V Risk. Risk during the high speed taxi test is minimal.

Appendix B: MATLAB® Data Reduction Scripts

B-1: PSI ESP Module Calibration Code

```
%------------------------
% Calibration Code for PSI ESP module voltages
%
% Drew Turner
%
% Test Day: 02/02/2005
% atm. pressure = 30.36 in Hg
%------------------------

% Applies 4th order polynomial calibration to the voltages recorded by
%  LIFT computer to obtain total pressures at engine inlet face.
%  Removes zero offset and outputs calibrated values to a new file.
% Pressure units: pounds per square inch

atmpressure= 30.36*0.4913;        % Conversion from inches of Hg
                                  %  to pounds per sq. in
                                  %<---Change For New Test Day!!!!
data_PSI_000
PSI_DATA000=PSI_DATA(:,2:end);

data_PSI_006                      %<---Change For New File!!!!
timePSI = PSI_DATA(:,1);
PSI_DATA = PSI_DATA(:,2:end);

[k,not2]=size(PSI_DATA);

load espcal

for i=1:40
    co(i)=espcal(i,2)*PSI_DATA000(:,i)+espcal(i,3)*PSI_DATA000(:,i)^2+...
        espcal(i,4)*PSI_DATA000(:,i)^3+espcal(i,5)*PSI_DATA000(:,i)^4;
end

for j=1:k
for i=1:40
    PSIcal(j,i)=(-1.0*co(i)+espcal(i,2)*PSI_DATA(j,i)+espcal(i,3)*...
        PSI_DATA(j,i)^2+espcal(i,4)*PSI_DATA(j,i)^3+espcal(i,5)*...
        PSI_DATA(j,i)^4+atmpressure);
end
end

c_data = fopen('data_PSI_006calib.m', 'w+'); %<--Change For New File!!!!

fprintf(c_data, '%% NCSU Flight Test Data for Test UAV \n');
fprintf(c_data, '%% Calibrated PSI DATA \n');
fprintf(c_data, '%% High Speed Taxi Test \n');
fprintf(c_data, ' \n');
fprintf(c_data, ' \n');
fprintf(c_data, 'PSI_DATA = [ \n');
```

```
for j=1:k
fprintf(c_data, ['%6.3f %7.6f %7.6f %7.6f %7.6f %7.6f %7.6f %7.6f'...
                 '%7.6f %7.6f %7.6f %7.6f %7.6f %7.6f %7.6f %7.6f'...
                 '%7.6f %7.6f %7.6f %7.6f %7.6f %7.6f %7.6f %7.6f'...
                 '%7.6f %7.6f %7.6f %7.6f %7.6f %7.6f %7.6f %7.6f'...
                 '%7.6f %7.6f %7.6f %7.6f %7.6f %7.6f %7.6f %7.6f'...
                 '%7.6f \n'], ...
                 [timePSI(j);PSIcal(j,1);PSIcal(j,2);PSIcal(j,3);...
                 PSIcal(j,4);PSIcal(j,5);PSIcal(j,6);PSIcal(j,7);...
                 PSIcal(j,8);PSIcal(j,9);PSIcal(j,10);PSIcal(j,11);...
                 PSIcal(j,12);PSIcal(j,13);PSIcal(j,14);PSIcal(j,15);...
                 PSIcal(j,16);PSIcal(j,17);PSIcal(j,18);PSIcal(j,19);...
                 PSIcal(j,20);PSIcal(j,21);PSIcal(j,22);PSIcal(j,23);...
                 PSIcal(j,24);PSIcal(j,25);PSIcal(j,26);PSIcal(j,27);...
                 PSIcal(j,28);PSIcal(j,29);PSIcal(j,30);PSIcal(j,31);...
                 PSIcal(j,32);PSIcal(j,33);PSIcal(j,34);PSIcal(j,35);...
                 PSIcal(j,36);PSIcal(j,37);PSIcal(j,38);PSIcal(j,39);...
                 PSIcal(j,40)]);
end

fprintf(c_data, ']; \n');

fclose(c_data);
```

B-2: Transducer Calibration File

```
%------------------------
% Calibration Code for XD Raw Data
%
% Drew Turner
%
% Test Day: 02/02/2005
% atm. pressure = 30.36 in Hg
%------------------------

% Applies Zero Offsets from Calibration Files (ex. DATA_XD_000.m)
% then outputs calibrated values to new file

% Count from the Calibration File_000
% Offset from Calibration File -- VoltageSlope*XDSlope*Count + XDZero

DATA_XD_000

% Dynamic Pressure offset
% units:  pounds per square inch (psi)
DynPress_ZeroCnt = XD_DATA(:,23);
DynPress_offset = 152.59e-6*DynPress_ZeroCnt*0.2447 - 0.1243;

% Static Pressure offset
% units: psi
Pstatic_ZeroCnt = XD_DATA(:,24);
Pstatic_offset = 152.59e-6*0.2418*Pstatic_ZeroCnt - 0.1223;

% Manifold Pressure 1 offset
% units: psi
Man1_ZeroCnt = XD_DATA(:,25);
Man1_offset = 152.59e-6*7.3300*Man1_ZeroCnt - 3.6890;

% Manifold Pressure 2 offset
% units: psi
Man2_ZeroCnt = XD_DATA(:,26);
Man2_offset = 152.59e-6*7.3400*Man2_ZeroCnt - 3.699;

% Angle of Attack offset
% units: radians
AOA_ZeroCnt = XD_DATA(:,27);
AOA_offset = 76.2951e-6*0.2143*AOA_ZeroCnt - 0.01209;

% Angle of Sideslip offset
% units: radians
AOS_ZeroCnt = XD_DATA(:,28);
AOS_offset = 76.2951e-6*(-0.1933)*AOS_ZeroCnt - 0.007309;

% Rotor Speed offset
% units: RPM x 1000
RPM_ZeroCnt = XD_DATA(:,29);
RPM_offset = 0.0;
```

```
DATA_XD_004                          %<---Change For New File!!!

Time = XD_DATA(:,1);              % Time (seconds)

% CVAs 1-12 Data Columns 2-13 (voltages)
CVA1 = XD_DATA(:,2);
CVA2 = XD_DATA(:,3);
CVA3 = XD_DATA(:,4);
CVA4 = XD_DATA(:,5);
CVA5 = XD_DATA(:,6);
CVA6 = XD_DATA(:,7);
CVA7 = XD_DATA(:,8);
CVA8 = XD_DATA(:,9);
CVA9 = XD_DATA(:,10);
CVA10 = XD_DATA(:,11);
CVA11 = XD_DATA(:,12);
CVA12 = XD_DATA(:,13);

% Avionics Battery Voltage
Batt_Volt = XD_DATA(:,14);

% Inertial Measurement Unit (IMU) Data
A_x = XD_DATA(:,15);                % Linear Acceleration in X-axis (Gs)
A_y = XD_DATA(:,16);                % Linear Acceleration in Y-axis (Gs)
A_z = XD_DATA(:,17);                % Linear Acceleration in Z-axis (Gs)
P = XD_DATA(:,18);                  % Roll Rate (radians per second)
Q = XD_DATA(:,19);                  % Pitch Rate (radians per second)
R = XD_DATA(:,20);                  % Yaw Rate (radians per second)
Phi = XD_DATA(:,23);                % Bank Angle (radians)
Theta = XD_DATA(:,22);              % Pitch Angle (radians)

% Pressure Data from mini air data boom (pounds per sq. in.)
DynPress_cal = XD_DATA(:,23) - DynPress_offset;
Pstatic_cal = XD_DATA(:,24) - Pstatic_offset;

% Manifold Pressures from Inlet (pounds per sq. in.)
Man1_cal = XD_DATA(:,25) - Man1_offset;
Man2_cal = XD_DATA(:,26) - Man2_offset;

% Data from min air dat boom
AOA_cal = XD_DATA(:,27) - AOA_offset;      % Angle of Attack (radians)
AOS_cal = XD_DATA(:,28) - AOS_offset;      % Angle of Sideslip (radians)

% RPM sensor data
RPM_cal = XD_DATA(:,29) - RPM_offset;        % Rotor Speed (RPM x 1000)


c_data = fopen('data_XD_004calib.m', 'w+');  %<---Change for New File!!!

fprintf(c_data, '%% NCSU Flight Test Data for Test UAV \n');
fprintf(c_data, '%% Calibrated XD DATA \n');
fprintf(c_data, '%% High Speed Taxi Test \n');
```

```
fprintf(c_data, ' \n');
fprintf(c_data, ' \n');
fprintf(c_data, 'XD_DATA = [ \n');
fprintf(c_data, ['%6.3f %7.6f %7.6f %7.6f %7.6f %7.6f %7.6f %7.6f'...
                 '%7.6f %7.6f %7.6f %7.6f %8.6f %8.6f %8.6f %8.6f'...
                 '%8.6f %8.6f %8.6f %8.6f %8.6f %8.6f %8.6f %8.6f'...
                 '%8.6f %8.6f %8.6f %8.6f %8.6f \n'], [Time(:)';...
                 CVA1(:)';CVA2(:)';CVA3(:)';CVA4(:)';CVA5(:)';...
                 CVA6(:)';CVA7(:)';CVA8(:)';CVA9(:)';CVA10(:)';...
                 CVA11(:)';CVA12(:)';Batt_Volt(:)';A_x(:)';A_y(:)';...
                 A_z(:)';P(:)';Q(:)';R(:)';Phi(:)';Theta(:)';...
                 DynPress_cal(:)';Pstatic_cal(:)';Man1_cal(:)';...
                 Man2_cal(:)';AOA_cal(:)';AOS_cal(:)';RPM_cal(:)']);
fprintf(c_data, ']; \n');

fclose(c_data);
```

B-3: Inlet Face Distortion and Takeoff Performance Analysis Script

```
%------------------------
% Data Reduction Code for UAV Taxi Tests
%
% Drew Turner
%
% Test Day: 02/02/2005
% atm. pressure = 30.36 in Hg
%------------------------


rho = 0.0023769;                              % Standard Density at sea
                                              % level in slugs per cubic foot

atmpressure= 30.36*0.4913;                    % Conversion from inches
                                              %  of Hg to pounds per sq. in.
                                              %<---Change For New Test Day!!!


time = fopen('375_flowonTime.dat','w');
inletPSI = fopen('375_flowonPSI.dat','w');   %<---Change For New File!!!
press_recov = fopen('375_flowonPressRecov.dat','w');
cdist1 = fopen('375_flowonCD1.dat','w');     %<---Change For New File!!!
cdist2 = fopen('375_flowonCD2.dat','w');     %<---Change For New File!!!
cdist3 = fopen('375_flowonCD3.dat','w');     %<---Change For New File!!!
cdist4 = fopen('375_flowonCD4.dat','w');     %<---Change For New File!!!
cdist5 = fopen('375_flowonCD5.dat','w');     %<---Change For New File!!!
cdistAll = fopen('375_flowonCD.dat','w');    %<---Change For New File!!!
cdist_ext = fopen('375_flowonCDExt.dat','w');
raddist_int = fopen('375_flowonRDInt.dat','w');
intelem = fopen('375_flowonIntElem.dat','w'); %<---Change For New File!!!
vel2file = fopen('375_flowonVel.dat','w');    %<---Change For New File!!!
totpressrec = fopen('375_flowonTotPressRec.dat','w');
manpress = fopen('375_flowonManPress.dat','w'); %<---Change For New
File!!!

data_PSI_006calib                             %<---Change For New File!!!
timePSI = PSI_DATA(:,1);
PSI_DATA = PSI_DATA(:,2:end);

[k,not2]=size(PSI_DATA);

data_XD_006calib                              %<---Change For New File!!!
timeXD = XD_DATA(:,1);
[n,not3] = size(XD_DATA);

data_RC_006

% Dynamic Pressure
%

dynpress = XD_DATA(:,23)*144;     % Dynamic Pressure in pounds per sq. ft.
```

```
for j=1:k
   if dynpress(j) > 0.0
        velocity(j) = (2*dynpress(j)/rho)^(1/2);  % Calculates velocity
   else                                           % in ft/sec from
        velocity(j) = 1e-6;                       % dynamic press.
   end
end

dynpress_avg = mean(dynpress(1:500));

dynpress_adj = 0.0003*10.0^2+0.0012*10.0+0.0017;
dynpress_avgcorr = dynpress_avg + dynpress_adj*dynpress_avg;

wind_vel = (2.0*dynpress_avgcorr/rho)^(1/2);

wind_angle = 10*pi/180;             % wind angle off of runway (radians)

v_y = wind_vel * sin(wind_angle);              % crosswind component
v_x = wind_vel * cos(wind_angle);              % headwind component

for j=1:k
    rat = v_y/velocity(j);
    if rat > 1
        rat = 1;
    end

    sideslip(j) = asin(rat);                  % sideslip angle (radians)
    sideslip_deg(j) = sideslip(j)*180/pi;     % sideslip angle (degrees)

    if sideslip_deg(j)>=0.0 && sideslip_deg(j)<=3.0
        per_corr(j)=0.0033*sideslip_deg(j);
    else
        per_corr(j)=0.0003*sideslip_deg(j)^2+0.0012*sideslip_deg(j)...
            +0.0017;
    end

    dynpress_corr(j)=dynpress(j)+per_corr(j)*dynpress(j);  % corrected
                                                           % dynamic press
                                                           % for sideslip

    if dynpress_corr(j) >0.0
        pressure(j) = (dynpress_corr(j)/144) + atmpressure;
        velocity_corr(j)=(2.0*dynpress_corr(j)/rho)^(1/2);
    else
        pressure(j) = atmpressure;
        velocity_corr(j) = 0.0;
    end

    v_x2 = velocity_corr(j)*cos(sideslip(j));       % aircraft ground
    velocity_corr2(j) = v_x2 - v_x;                 % speed
                                                    % (headwind removed)

end
```

```
man1 = XD_DATA(:,25);
man2 = XD_DATA(:,26);

throttle = RC_DATA(2:end,6);
throttle_max = max(throttle);
throttle_min = min(throttle);

for v=1:k-1
throttle(v) = (throttle(v)-throttle_min)/(throttle_max-throttle_min);
end

% Grid and Inlet Rake Layout

x = [0,0.4375,0.6204,0.4375,0,-0.4375,-0.6204,-0.4375,0,0.7819,1.1074,...
     0.7819,0,-0.7819,-1.1074,-0.7819,0,0.9796,1.3870,0.9796,0,-0.9796,...
     -1.3870,-0.9796,0,1.1596,1.6415,1.1596,0,-1.1596,-1.6415,-1.1596,...
     0,1.3151,1.8615,1.3151,0,-1.3151,-1.8615,-1.3151];
z = [0.6204,0.4398,0,-0.4398,-0.6204,-0.4398,0,0.4398,1.1074,0.7842,0,...
     -0.7842,-1.1074,-0.7842,0,0.7842,1.3870,0.9819,0,-0.9819,-1.3870,...
     -0.9819,0,0.9819,1.6415,1.1618,0,-1.1618,-1.6415,-1.1618,0,1.1618,...
     1.8615,1.3174,0,-1.3174,-1.8615,-1.3174,0,1.3174];

theta = [-135,-90,-45,0,45,90,135,180];

grid1 = [1,8,7,6,5,4,3,2,9,16,15,14,13,12,11,10,17,24,23,22,21,20,19,...
         18,25,32,31,30,29,28,27,26,5,5,1];
grid2 = [8,7,6,5,4,3,2,1,16,15,14,13,12,11,10,9,24,23,22,21,20,19,18,...
         17,32,31,30,29,28,27,26,25,6,8,2];
grid3 = [16,15,14,13,12,11,10,9,24,23,22,21,20,19,18,17,32,31,30,29,28,...
         27,26,25,40,39,38,37,36,35,34,33,7,1,3];
grid4 = [9,16,15,14,13,12,11,10,17,24,23,22,21,20,19,18,25,32,31,30,29,...
         28,27,26,33,40,39,38,37,36,35,34,8,4,4];

counter=0.0;
fprintf(time,'No.     Time \n');

fprintf(intelem,'TITLE   = "High Speed Taxi Test 02/02/05" \n');
fprintf(intelem,'VARIABLES = "Time" "Ring 1" "Ring 2" "Ring 3"'...
                '"Ring 4" "Ring 5" "Total Int" \n');

for j=1:k
%for j=1:3:k

    counter = counter + 1.0;

    PSI_DATA(j,9)=(PSI_DATA(j,1) + PSI_DATA(j,17))/2.0;  % Average two
                                                         % ports above
                                                         % and below
                                                         % blocked port

for i=1:40
    PressRecov(j,i)=PSI_DATA(j,i)/pressure(j);
```

```
end

% Radial Distortion

    ring1=PSI_DATA(j,1:8);
    ring2=PSI_DATA(j,9:16);
    ring3=PSI_DATA(j,17:24);
    ring4=PSI_DATA(j,25:32);
    ring5=PSI_DATA(j,33:40);

    pav1=sum(ring1)/8;  % Ring Average Total Pressure per sample time
    pav2=sum(ring2)/8;
    pav3=sum(ring3)/8;
    pav4=sum(ring4)/8;
    pav5=sum(ring5)/8;

    pfav=(pav1+pav2+pav3+pav4+pav5)/5;  % Face Average Total Pressure
                                        % per sample time

    total_PressRecov(j)=pfav/atmpressure;  % Overall Pressure recovery


    a1(j)=(pfav-pav1)/pfav;  %Radial Distortion Intensity Element - Ring 1
    a2(j)=(pfav-pav2)/pfav;  %Radial Distortion Intensity Element - Ring 2
    a3(j)=(pfav-pav3)/pfav;  %Radial Distortion Intensity Element - Ring 3
    a4(j)=(pfav-pav4)/pfav;  %Radial Distortion Intensity Element - Ring 4
    a5(j)=(pfav-pav5)/pfav;  %Radial Distortion Intensity Element - Ring 5



% Circumferential Distortion

CircDist_ExtRing1           % Calls script to calculate circumferential
CircDist_ExtRing2           % distortion extent element
CircDist_ExtRing3
CircDist_ExtRing4
CircDist_ExtRing5

    sum1=0;
    sum2=0;
    sum3=0;
    sum4=0;
    sum5=0;

    count1=0;
    count2=0;
    count3=0;
    count4=0;
    count5=0;

    for g=1:8
        if ring1(g)<pav1;
            sum1=ring1(g)+sum1;
```

```
        count1=count1+1;
    end

    if count1==0.0;
        pavlow1=0.0;
    else
        pavlow1=sum1/count1;
    end

    if ring2(g)<pav2;
        sum2=ring2(g)+sum2;
        count2=count2+1;
    end

    if count2==0.0;
        pavlow2=0.0;
    else
        pavlow2=sum2/count2;
    end

    if ring3(g)<pav3;
        sum3=ring3(g)+sum3;
        count3=count3+1;
    end

    if count3==0.0;
        pavlow3=0.0;
    else
        pavlow3=sum3/count3;
    end

    if ring4(g)<pav4;
        sum4=ring4(g)+sum4;
        count4=count4+1;
    end

    if count4==0.0;
        pavlow4=0.0;
    else
        pavlow4=sum4/count4;
    end

    if ring5(g)<pav5;
        sum5=ring5(g)+sum5;
        count5=count5+1;
    end

    if count5==0.0;
        pavlow5=0.0;
    else
        pavlow5=sum5/count5;
    end
end
```

```
b1=(pav1-pavlow1)/pav1; %DCPC:  Circumferential Distortion intensity
                        %       element for Ring 1
b2=(pav2-pavlow2)/pav2; %DCPC:  Circumferential Distortion intensity
                        %       element for Ring 2
b3=(pav3-pavlow3)/pav3; %DCPC:  Circumferential Distortion intensity
                        %       element for Ring 3
b4=(pav4-pavlow4)/pav4; %DCPC:  Circumferential Distortion intensity
                        %       element for Ring 4
b5=(pav5-pavlow5)/pav5; %DCPC:  Circumferential Distortion intensity
                        %       element for Ring 5

total_dist(j)=(b1+b2+b2+b3+b4+b5)/5;

fprintf(time,'%7.6f %7.6f \n',[counter;timePSI(j)]);

% Outputs to file for Tecplot

% 1. Pressure Recovery Plots

fprintf(inletPSI,'TITLE   = "High Speed Taxi Test 02/02/05" \n');
fprintf(inletPSI,'VARIABLES = "X", "Z", "PressRecov" \n');
fprintf(inletPSI,'ZONE N=40, e=35, F=fepoint, et=quadrilateral \n');
fprintf(inletPSI,'%7.6f %7.6f %7.6f \n',[x;z;PressRecov(j,:)]);
fprintf(inletPSI,'%3.0f \t %3.0f \t %3.0f \t %3.0f \n',...
                 [grid1;grid2;grid3;grid4]);

fprintf(press_recov,'%7.6f %7.6f %7.6f %7.6f %7.6f %7.6f %7.6f'...
                    '%7.6f %7.6f %7.6f %7.6f %7.6f %7.6f %7.6f'...
                    '%7.6f %7.6f %7.6f %7.6f %7.6f %7.6f %7.6f'...
                    '%7.6f %7.6f %7.6f %7.6f %7.6f %7.6f %7.6f'...
                    '%7.6f %7.6f %7.6f %7.6f %7.6f %7.6f %7.6f'...
                    '%7.6f %7.6f %7.6f %7.6f %7.6f %7.6f \n', ...
                [timePSI(j);PressRecov(j,1);PressRecov(j,2);...
                PressRecov(j,3);PressRecov(j,4);PressRecov(j,5);...
                PressRecov(j,6);PressRecov(j,7);PressRecov(j,8);...
                PressRecov(j,9);PressRecov(j,10);PressRecov(j,11);...
                PressRecov(j,12);PressRecov(j,13);PressRecov(j,14);...
                PressRecov(j,15);PressRecov(j,16);PressRecov(j,17);...
                PressRecov(j,18);PressRecov(j,19);PressRecov(j,20);...
                PressRecov(j,21);PressRecov(j,22);PressRecov(j,23);...
                PressRecov(j,24);PressRecov(j,25);PressRecov(j,26);...
                PressRecov(j,27);PressRecov(j,28);PressRecov(j,29);...
                PressRecov(j,30);PressRecov(j,31);PressRecov(j,32);...
                PressRecov(j,33);PressRecov(j,34);PressRecov(j,35);...
                PressRecov(j,36);PressRecov(j,37);PressRecov(j,38);...
                PressRecov(j,39);PressRecov(j,40);]);

% 2. Circumferential Distortion Pattern Plots

% Ring 1
    fprintf(cdist1,'TITLE   = "High Speed Taxi Test 02/02/05" \n');
    fprintf(cdist1,'VARIABLES = "Theta", "TotPress", "AvgPress" \n');
    fprintf(cdist1,'ZONE I = 8, F=point \n',j);
```

```
    fprintf(cdist1,'%7.6f %7.6f %7.6f \n',[theta(1);ring1(6);pav1]);
    fprintf(cdist1,'%7.6f %7.6f %7.6f \n',[theta(2);ring1(7);pav1]);
    fprintf(cdist1,'%7.6f %7.6f %7.6f \n',[theta(3);ring1(8);pav1]);
    fprintf(cdist1,'%7.6f %7.6f %7.6f \n',[theta(4);ring1(1);pav1]);
    fprintf(cdist1,'%7.6f %7.6f %7.6f \n',[theta(5);ring1(2);pav1]);
    fprintf(cdist1,'%7.6f %7.6f %7.6f \n',[theta(6);ring1(3);pav1]);
    fprintf(cdist1,'%7.6f %7.6f %7.6f \n',[theta(7);ring1(4);pav1]);
    fprintf(cdist1,'%7.6f %7.6f %7.6f \n',[theta(8);ring1(5);pav1]);

% Ring 2
    fprintf(cdist2,'TITLE   = "High Speed Taxi Test 02/02/05" \n');
    fprintf(cdist2,'VARIABLES = "Theta", "TotPress", "AvgPress" \n');
    fprintf(cdist2,'ZONE I = 8, F=point \n',j);
    fprintf(cdist2,'%7.6f %7.6f %7.6f \n',[theta(1);ring2(6);pav2]);
    fprintf(cdist2,'%7.6f %7.6f %7.6f \n',[theta(2);ring2(7);pav2]);
    fprintf(cdist2,'%7.6f %7.6f %7.6f \n',[theta(3);ring2(8);pav2]);
    fprintf(cdist2,'%7.6f %7.6f %7.6f \n',[theta(4);ring2(1);pav2]);
    fprintf(cdist2,'%7.6f %7.6f %7.6f \n',[theta(5);ring2(2);pav2]);
    fprintf(cdist2,'%7.6f %7.6f %7.6f \n',[theta(6);ring2(3);pav2]);
    fprintf(cdist2,'%7.6f %7.6f %7.6f \n',[theta(7);ring2(4);pav2]);
    fprintf(cdist2,'%7.6f %7.6f %7.6f \n',[theta(8);ring2(5);pav2]);

% Ring 3
    fprintf(cdist3,'TITLE   = "High Speed Taxi Test 02/02/05" \n');
    fprintf(cdist3,'VARIABLES = "Theta", "TotPress", "AvgPress" \n');
    fprintf(cdist3,'ZONE I = 8, F=point \n',j);
    fprintf(cdist3,'%7.6f %7.6f %7.6f \n',[theta(1);ring3(6);pav3]);
    fprintf(cdist3,'%7.6f %7.6f %7.6f \n',[theta(2);ring3(7);pav3]);
    fprintf(cdist3,'%7.6f %7.6f %7.6f \n',[theta(3);ring3(8);pav3]);
    fprintf(cdist3,'%7.6f %7.6f %7.6f \n',[theta(4);ring3(1);pav3]);
    fprintf(cdist3,'%7.6f %7.6f %7.6f \n',[theta(5);ring3(2);pav3]);
    fprintf(cdist3,'%7.6f %7.6f %7.6f \n',[theta(6);ring3(3);pav3]);
    fprintf(cdist3,'%7.6f %7.6f %7.6f \n',[theta(7);ring3(4);pav3]);
    fprintf(cdist3,'%7.6f %7.6f %7.6f \n',[theta(8);ring3(5);pav3]);

% Ring 4
    fprintf(cdist4,'TITLE   = "High Speed Taxi Test 02/02/05" \n');
    fprintf(cdist4,'VARIABLES = "Theta", "TotPress", "AvgPress" \n');
    fprintf(cdist4,'ZONE I = 8, F=point \n',j);
    fprintf(cdist4,'%7.6f %7.6f %7.6f \n',[theta(1);ring4(6);pav4]);
    fprintf(cdist4,'%7.6f %7.6f %7.6f \n',[theta(2);ring4(7);pav4]);
    fprintf(cdist4,'%7.6f %7.6f %7.6f \n',[theta(3);ring4(8);pav4]);
    fprintf(cdist4,'%7.6f %7.6f %7.6f \n',[theta(4);ring4(1);pav4]);
    fprintf(cdist4,'%7.6f %7.6f %7.6f \n',[theta(5);ring4(2);pav4]);
    fprintf(cdist4,'%7.6f %7.6f %7.6f \n',[theta(6);ring4(3);pav4]);
    fprintf(cdist4,'%7.6f %7.6f %7.6f \n',[theta(7);ring4(4);pav4]);
    fprintf(cdist4,'%7.6f %7.6f %7.6f \n',[theta(8);ring4(5);pav4]);

% Ring 5
    fprintf(cdist5,'TITLE   = "High Speed Taxi Test 02/02/05" \n');
    fprintf(cdist5,'VARIABLES = "Theta", "TotPress", "AvgPress" \n');
    fprintf(cdist5,'ZONE I = 8, F=point \n',j);
    fprintf(cdist5,'%7.6f %7.6f %7.6f \n',[theta(1);ring5(6);pav5]);
    fprintf(cdist5,'%7.6f %7.6f %7.6f \n',[theta(2);ring5(7);pav5]);
    fprintf(cdist5,'%7.6f %7.6f %7.6f \n',[theta(3);ring5(8);pav5]);
```

```
        fprintf(cdist5,'%7.6f %7.6f %7.6f \n',[theta(4);ring5(1);pav5]);
        fprintf(cdist5,'%7.6f %7.6f %7.6f \n',[theta(5);ring5(2);pav5]);
        fprintf(cdist5,'%7.6f %7.6f %7.6f \n',[theta(6);ring5(3);pav5]);
        fprintf(cdist5,'%7.6f %7.6f %7.6f \n',[theta(7);ring5(4);pav5]);
        fprintf(cdist5,'%7.6f %7.6f %7.6f \n',[theta(8);ring5(5);pav5]);

    % All Rings
        fprintf(cdistAll,'TITLE   = "High Speed Taxi Test 02/02/05" \n');
        fprintf(cdistAll,'VARIABLES = "Theta", "Ring 1", "Ring 2",'...
                         '"Ring 3", "Ring 4", "Ring 5" \n');
        fprintf(cdistAll,'ZONE I = 8, F=point \n',j);
        fprintf(cdistAll,'%7.6f %7.6f %7.6f \n',...
                [theta(1);ring1(6);ring2(6);ring3(6);ring4(6);ring5(6)]);
        fprintf(cdistAll,'%7.6f %7.6f %7.6f \n',...
                [theta(2);ring1(7);ring2(7);ring3(7);ring4(7);ring5(7)]);
        fprintf(cdistAll,'%7.6f %7.6f %7.6f \n',...
                [theta(3);ring1(8);ring2(8);ring3(8);ring4(8);ring5(8)]);
        fprintf(cdistAll,'%7.6f %7.6f %7.6f \n',...
                [theta(4);ring1(1);ring2(1);ring3(1);ring4(1);ring5(1)]);
        fprintf(cdistAll,'%7.6f %7.6f %7.6f \n',...
                [theta(5);ring1(2);ring2(2);ring3(2);ring4(2);ring5(2)]);
        fprintf(cdistAll,'%7.6f %7.6f %7.6f \n',...
                [theta(6);ring1(3);ring2(3);ring3(3);ring4(3);ring5(3)]);
        fprintf(cdistAll,'%7.6f %7.6f %7.6f \n',...
                [theta(7);ring1(4);ring2(4);ring3(4);ring4(4);ring5(4)]);
        fprintf(cdistAll,'%7.6f %7.6f %7.6f \n',...
                [theta(8);ring1(5);ring2(5);ring3(5);ring4(5);ring5(5)]);

    % 3. Circumferential Distortion Intensity Elements
        fprintf(intelem,'%7.6f %7.6f %7.6f %7.6f %7.6f %7.6f %7.6f \n',...
                [timePSI(j);b1;b2;b3;b4;b5;total_dist(j)]);

    % 4. Circumferential Distortion Extent Elements
        fprintf(cdist_ext,'%7.6f %7.6f %7.6f %7.6f %7.6f %7.6f \n',...
                [timePSI(j);CircDistExt1;CircDistExt2;CircDistExt3;...
                 CircDistExt4;CircDistExt5]);

    % 5. Radial Distortion Extent Elements
        fprintf(raddist_int,'%7.6f %7.6f %7.6f %7.6f %7.6f %7.6f \n',...
                [timePSI(j);a1(j);a2(j);a3(j);a4(j);a5(j)]);

end

fclose(time);
fclose(inletPSI);
fclose(press_recov);
fclose(cdist1);
fclose(cdist2);
fclose(cdist3);
fclose(cdist4);
fclose(cdist5);
fclose(cdistAll);
fclose(cdist_ext);
fclose(raddist_int);
```

```
fclose(intelem);

%****************************************
%
% Integrate Acceleration in X-direction
%  from Crossbow to compare to velocity
%  from pitot-static boom

A_x = -1.0*XD_DATA(:,15);           % A_x in Gs

A_x = A_x * 32.2;                   % A_x in feet per second squared

% Adjusted A_x

%c = 620;        %---> 250 ft Run Flow Off - File 005!!!
%u = 2070;
%off1 = 0.241100147;
%off2 = 0.197032138;

%c = 725;        %---> 250 ft Run Flow On - File 004!!!
%u = 2217;
%off1 = 0.341471437;
%off2 = 0.435216895;

c= 650;        %---> 375 ft Run Flow On - File 006!!!
u= 2415;
off1 = 0.520725487;
off2 = 0.118934884;

A_x3 = A_x;

for d=1:c
    A_x3(d) = A_x(d) - off1;
end

for t=u:k
    A_x3(t) = A_x(t) - off2;
end


delta_t = 0.02;                 % Sampling rate of 50 Hz = 0.02 seconds

Xbow_vel(1) = A_x(1)*delta_t;
Xbow_vel3(1) = A_x3(1)*delta_t;

Xbow_dist(1) = Xbow_vel(1)*delta_t;
Xbow_dist3(1) = Xbow_vel3(1)*delta_t;

for m=2:1:n
    Xbow_vel(m) = A_x(m)*delta_t + Xbow_vel(m-1);
    Xbow_vel3(m) = A_x3(m)*delta_t + Xbow_vel3(m-1);
```

```
    Xbow_dist(m) = Xbow_vel(m)*delta_t + Xbow_dist(m-1);
    Xbow_dist3(m) = Xbow_vel3(m)*delta_t + Xbow_dist3(m-1);
end

fprintf(vel2file,'TITLE = "High Speed Taxi Test 02/02/05" \n');
fprintf(vel2file,['VARIABLES = "Time006", "Velocity006",'...
                             '"Velocity_corr006","Velocity_corr2006",'...
                             ' "Xbow_Vel006", "Xbow_Vel3006",'...
                             ' "A_x006", "A_x3006",'...
                             ' "Xbow_Dist006", "Xbow_Dist3006" \n']);

for l=1:k-1
    fprintf(vel2file,['%7.6f %7.6f %7.6f %7.6f %7.6f %7.6f %7.6f %7.6f'...
                      '%7.6f %7.6f %7.6f %7.6f %7.6f \n'],...
                     [timeXD(l);velocity(l);velocity_corr(l);...
                     velocity_corr2(l);...
                     Xbow_vel(l);Xbow_vel3(l);...
                     A_x(l);A_x3(l);...
                     Xbow_dist(l);Xbow_dist3(l)]);
end

fclose(vel2file);

%****************************************
%
% Total Pressure Recovery output file

fprintf(totpressrec,'TITLE = "High Speed Taxi Test 02/02/05" \n');
fprintf(totpressrec,'VARIABLES = "Time006", "Tot_PressRec006",'
                    '"Throttle006" \n');       %<---Change File Number
fprintf(totpressrec,'%7.6f %7.6f %7.6f \n',[timePSI(2:k)';...
                    total_PressRecov(2:k);throttle(1:k-1)']);

fclose(totpressrec);

%****************************************
%
% Manifold Pressure output file

fprintf(manpress,'TITLE = "High Speed Taxi Test 02/02/05" \n');
fprintf(manpress,'VARIABLES = "Time006", "man1006", "man2006",'...
                              '"Throttle006" \n');%<---Change File Number
fprintf(manpress,'%7.6f %7.6f %7.6f %7.6f \n',[timeXD(2:k)';man1(2:k)';...
                                        man2(2:k)';throttle(1:k-1)']);

fclose(manpress);
```

Appendix C: UAV Taxi Test Log

UAV Taxi Test Log

Test Day Conditions:

Date: February 2, 2005

Test Facility: Harnett County Airport

Vehicle Weight: 214 lbs

Temperature: 50° F

Atmospheric Pressure: 30.36 in Hg

Winds: 040 @ 7 knots

Test Plan:

Four high speed taxi runs collecting data for inlet flow distortion and takeoff performance analysis.

Test Events:

File No.	Run	Flow Control	Comment
000	Calibration	-	
001	CVA Calibration	-	
002	Static	Off	
003	Static	On	
004	250 ft	On	
005	250 ft	Off	
006	375 ft	On	Un-commanded Aileron Throw – Test Terminated
007			
008			
009			

Notes:
Aircraft antenna cable came loose from mount and sheathing melted to exhaust pipe. Aileron throw was part aircraft preprogrammed fail safe due to loss of signal between transmitter and receiver.

Appendix D: Additional Circumferential Distortion Pattern Plots

D-1: Static

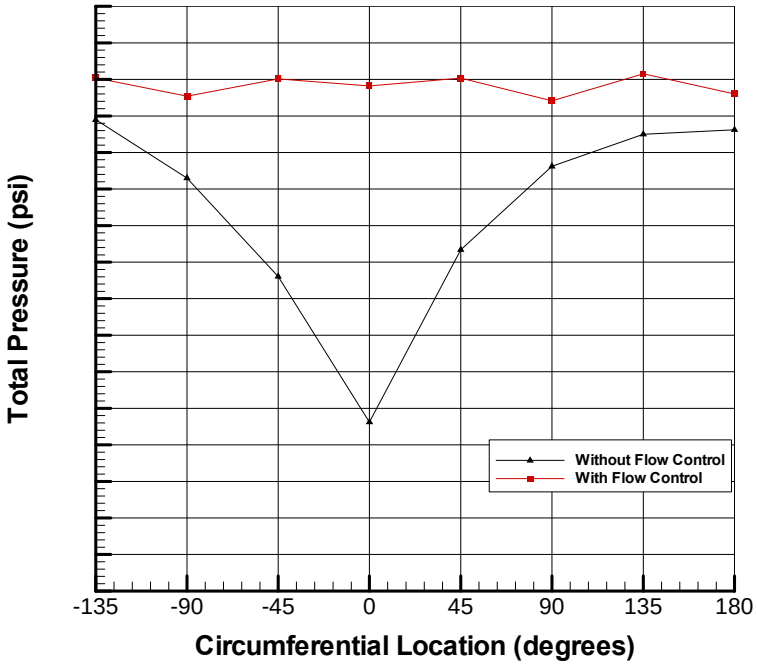

Comparison of Ring 1 Circumferential Distortion Pattern With and Without Flow Control

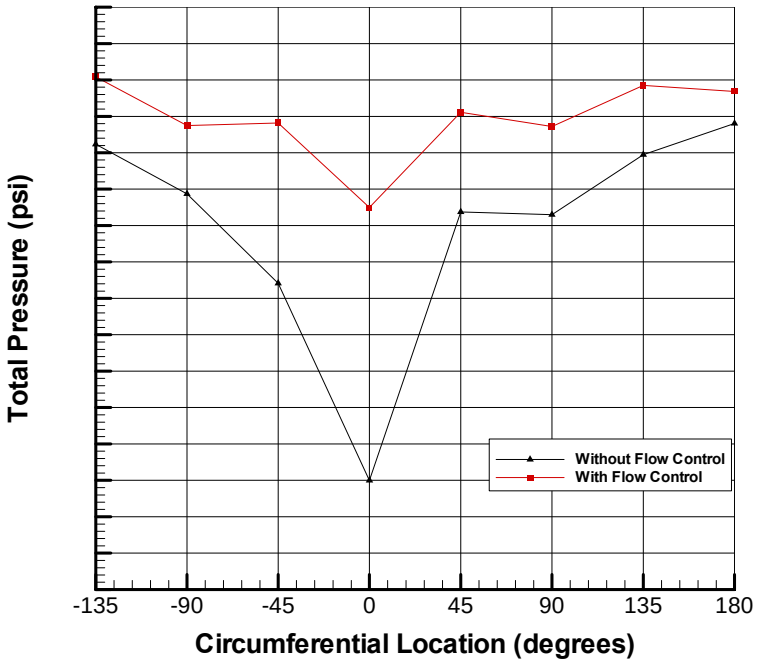

Comparison of Ring 2 Circumferential Distortion Pattern With and Without Flow Control

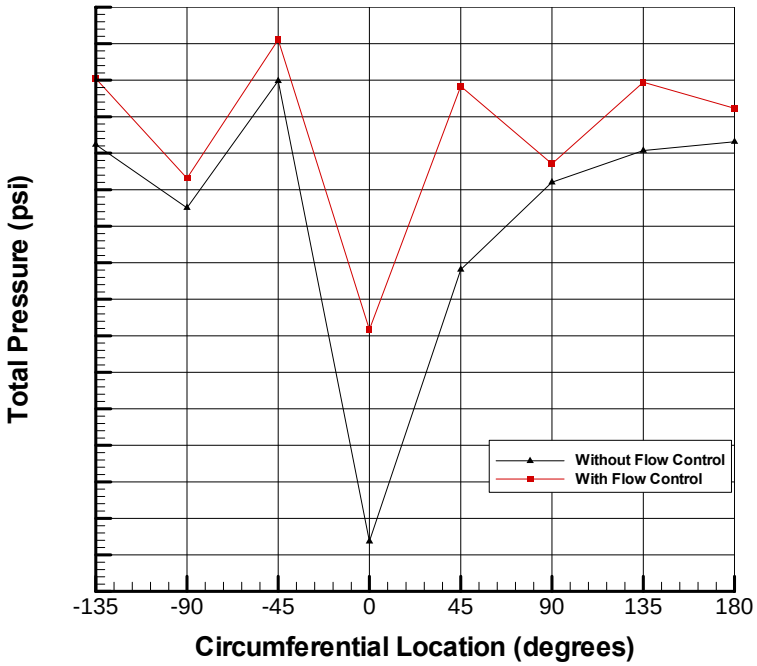

Comparison of Ring 3 Circumferential Distortion Pattern With and Without Flow Control

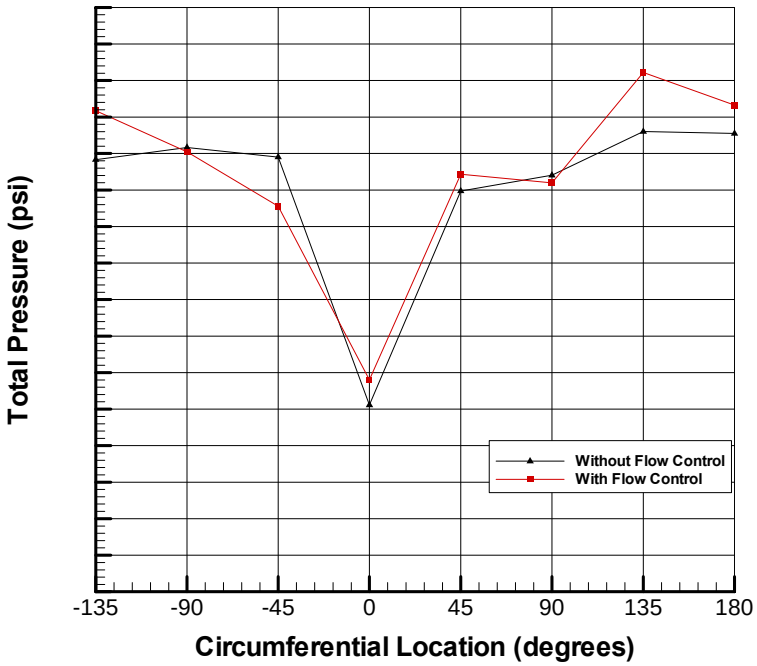

Comparison of Ring 4 Circumferential Distortion Pattern With and Without Flow Control

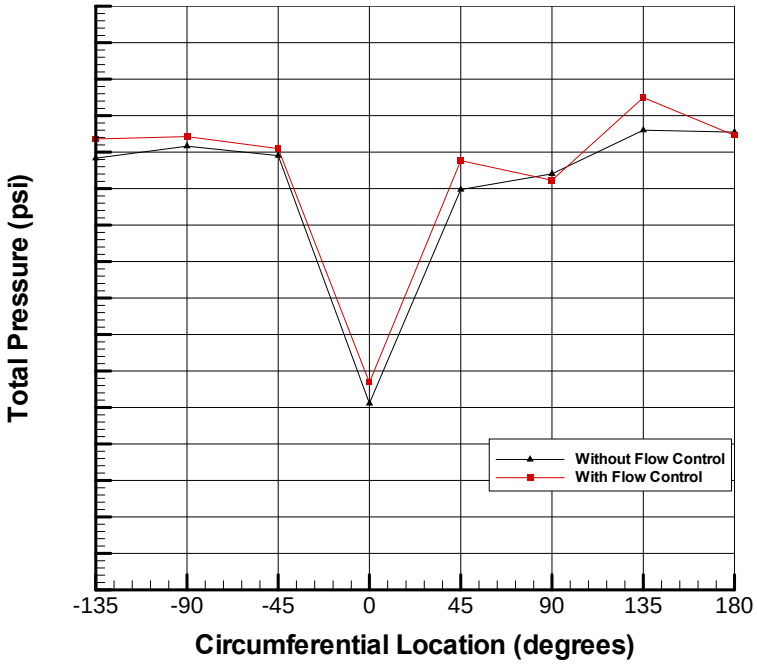

Comparison of Ring 5 Circumferential Distortion Pattern With and Without Flow Control

D-2: Dynamic – 250 ft Runs

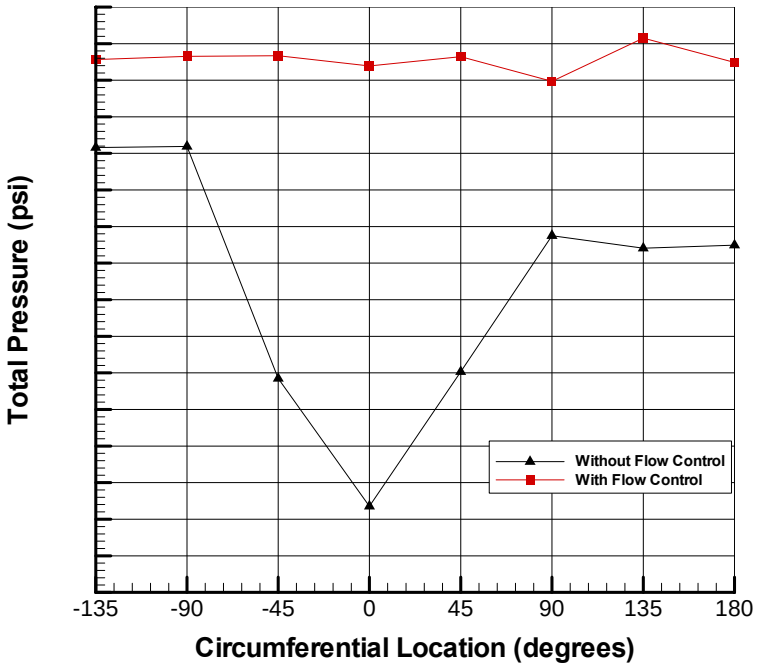

Comparison of Ring 1 Circumferential Distortion Pattern With and Without Flow Control

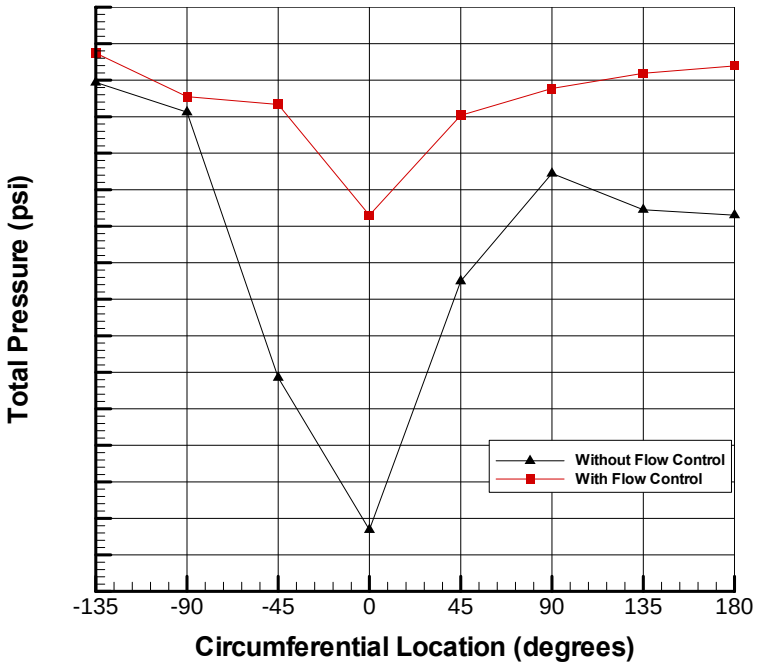

Comparison of Ring 2 Circumferential Distortion Pattern With and Without Flow Control

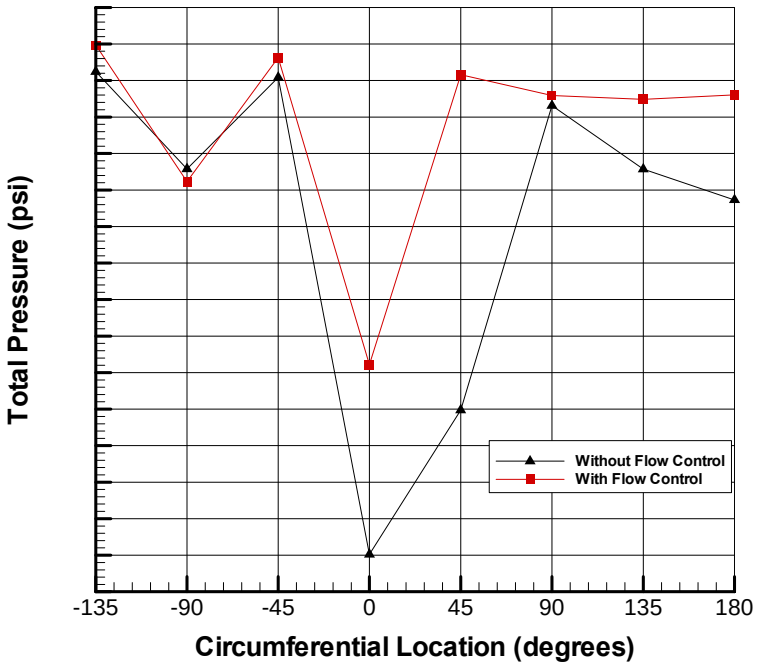

Comparison of Ring 3 Circumferential Distortion Pattern With and Without Flow Control

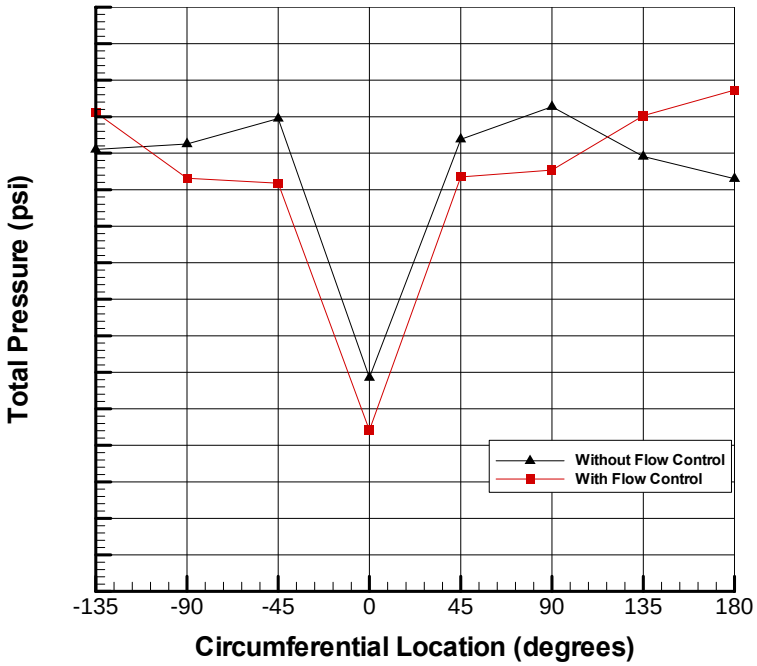

Comparison of Ring 4 Circumferential Distortion Pattern With and Without Flow Control

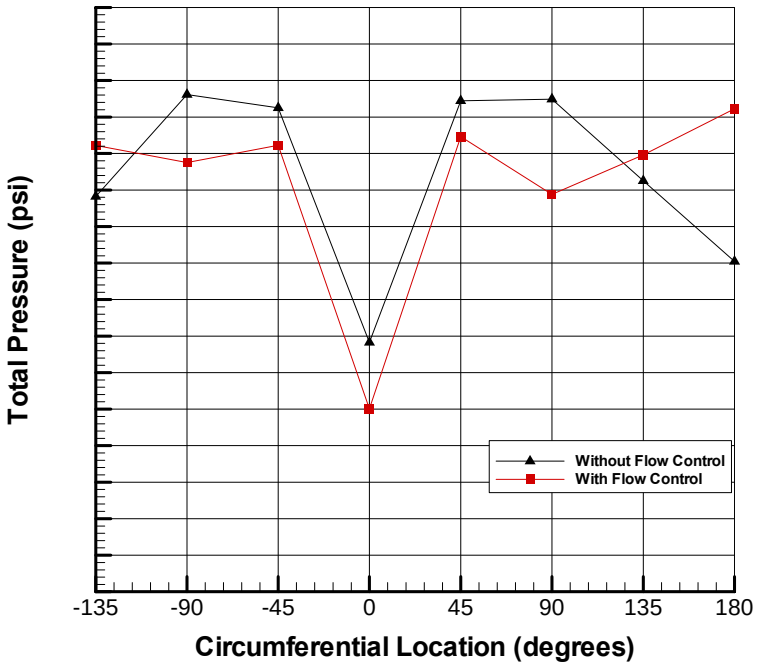

Comparison of Ring 5 Circumferential Distortion Pattern With and Without Flow Control